machines

MDPI

Article

Differential Flatness-Based Model Predictive Speed Control for Direct Current Motor–Gearhead Drive Systems

Elizabeth Delgadillo-Perez [1,2], Hugo Yañez-Badillo [2], Carlos Sotelo [3], David Sotelo [3], Francisco Beltran-Carbajal [1,*] and Jesus C. Hernandez [4,*]

1 Departamento de Energía, Unidad Azcapotzalco, Universidad Autónoma Metropolitana, Azcapotzalco, Mexico City 02200, Mexico; al2232800361@azc.uam.mx
2 Departamento de Investigación, Tecnológico Nacional de México: TES Tianguistenco, Tianguistenco 52650, Mexico State, Mexico; hugo_mecatronica@test.edu.mx
3 Tecnologico de Monterrey, Escuela de Ingeniería y Ciencias, Ave. Eugenio Garza Sada 2501 Sur, Col. Tecnológico, Monterrey 64700, N.L., Mexico; carlos.sotelo@tec.mx (C.S.); david.sotelo@tec.mx (D.S.)
4 Department of Electrical Engineering, University of Jaén, Campus Lagunillas s/n, Edificio A3, 23071 Jaen, Spain
* Correspondence: fbeltran@azc.uam.mx (F.B.-C.); jcasa@ujaen.es (J.C.H.)

Abstract

This paper introduces a new speed control framework design for direct current electric motors coupled with a gearhead. The proposed framework suitably integrates differential flatness, model predictive control, and Kalman filter theory for efficient speed tracking in disturbed scenarios. The performance of the proposed control framework is compared against a flat feed-forward proportional–integral–derivative controller, an extended state offset-free model predictive control, and a linear quadratic integral controller. The results show improved tracking performance with reductions of up to 60% in NRMSE and 50% in ITAE compared to the baseline controllers while maintaining a comparable and bounded control effort due to the constraints enforced in the framework formulation. These results show that the proposed approach effectively captures the dominant disturbance behaviour under varying operating conditions. Thus, it is demonstrated that the flat system formulation allows for proper speed control, providing practical insights for advanced motor control in industrial automation, robotics, and electric mobility applications.

Keywords: differential flatness; direct current electric motor; disturbance compensation; drive system; gearhead; Kalman filter; model predictive control

1. Introduction

Electric motors are widely used in industrial automation, robotics, and electric mobility applications where precise speed regulation and disturbance rejection are required. Among them, direct current (DC) motors are particularly valued in industry and domestic applications for their simplicity, efficiency, and ease of control in tasks requiring precise and fast motion [1–4].

In many practical applications, DC motors are mechanically coupled with gearhead transmissions, forming a DC motor–gearhead drive system capable of meeting high-torque requirements [5]. However, this configuration introduces additional mechanical challenges such as friction and backlash, that may degrade motion accuracy during real-time operation. Under these conditions, conventional control strategies often struggle to properly handle disturbances, actuator limits, and time-varying trajectories, highlighting an open research area.

Academic Editors: Mahmoud A. Mossa and Chojaa Hamid

Received: 31 March 2026
Revised: 1 May 2026
Accepted: 7 May 2026
Published: 12 May 2026

 https://doi.org/10.3390/machines14050542

On the other hand, model predictive control (MPC) is a control strategy that is useful in handling multivariable processes. This method consists of an optimal control technique that calculates the necessary inputs of a model to minimize its cost function, which represents its system dynamics using its constraints over a limited time horizon [6]. Based on this, MPC is a robust control technique which allows achieving improved tracking performance in applications where system dynamics, operational limits, and external disturbances play a critical role.

MPC has shown a great capacity to achieve a precise speed regulation in alternating current machines, taking advantage of its predictive nature to effectively manage system restrictions [7–9]. Despite the fact that its implementation may require a greater computational effort, it is considered a promising strategy for applications that require advanced speed control [10].

MPC has also demonstrated strong performance in the speed regulation of brushed DC motors, achieving overshoot-free responses and low steady-state error through appropriate cost function design [11]. Beyond brushed machines, predictive control strategies have also been successfully applied to permanent-magnet brushless DC motors, where they provide improved current regulation and reduced torque ripple compared to conventional feedback approaches [12]. Despite the differences in commutation mechanisms and dynamic characteristics, these studies highlight MPC as a flexible and effective control framework for electric motor drives.

As recognized in the literature, even when an accurate nominal model is available, unmodelled dynamics and external disturbances make it difficult to precisely represent real system behaviour. Since MPC performance strongly depends on model fidelity, this interaction often degrades its effectiveness in practical applications [13].

Several studies have proposed MPC combined with advanced techniques to control diverse complex systems. However, the treatment of external disturbances, unmodelled dynamics, and system uncertainties is addressed from different perspectives across the literature. Nevertheless, none of the reviewed works explicitly address disturbed DC motor–gearhead drive systems.

Some approaches enhance MPC performance by incorporating learning-based models that provide information on disturbances to the predictive controller. In these works, disturbances are indirectly characterized through data-driven representations integrated into the MPC framework. In [14], artificial neural networks were employed to learn the model–plant mismatch, from which disturbance information is derived and incorporated into the finite-horizon optimal control problem within an offset-free MPC framework. Similarly, in [15], a neural network-based MPC was proposed for output tracking control of a robotic arm, where the learned model provides the predictive dynamics and an extended state observer estimates the total disturbance acting on this data-driven representation.

The work in [16] integrated MPC with a long short-term memory network model. A modified observer, derived from the incremental stability properties of the network, is employed to estimate both the system states and disturbances which are incorporated into the MPC formulation to eliminate steady-state offset. In [17], a Gaussian process-based MPC scheme was introduced together with an extended state observer to estimate unmodelled dynamics and unknown disturbances. The Gaussian process captures the unknown system behaviour, while its expected variance is explicitly incorporated into the MPC formulation compensating for model uncertainty and enhance disturbance rejection.

In contrast to learning-based approaches, the present work does not rely on data-driven models to characterize disturbances. Instead, disturbance treatment is derived directly from the physical dynamics of the motor–gearhead drive system.

Other contributions rely on disturbance observers to explicitly estimate unknown dynamics and external perturbations, which are then incorporated into the MPC formulation through compensation terms, model corrections, or feed-forward actions. In [18], an extended-state observer was coupled with an ultra-local current model for interior permanent magnet synchronous motor systems. Here, parametric uncertainty, nonlinearities, and harmonic terms are lumped into a total disturbance term which is estimated online by the observer and incorporated as feed-forward compensation. Similarly, in [19], an offset-free MPC strategy was combined with a Koopman operator to derive a linear representation of complex soft manipulator dynamics, which is then implemented within a Kalman filter for disturbance estimation purposes.

The work in [20] proposed a disturbance rejection MPC scheme for a non-holonomic mobile robot that injects the disturbance estimate as an external compensation term after the MPC optimization, while the predictive model remains based on nominal dynamics. A related approach was presented in [21] for magnetic levitation control. Here, an equivalent input disturbance observer provides lumped disturbance estimates that are directly incorporated into the MPC prediction model as instantaneous correction term.

Conversely to these MPC observer-based strategies, which typically treat disturbances as quasi-stationary or slowly varying lumped signals, the proposed approach models disturbance behaviour through a polynomial representation. We explicitly consider their temporal evolution derived from the flat system dynamics and integrate it directly into the MPC prediction framework.

From a different research perspective, some papers assume that the inherent receding-horizon nature of MPC provides sufficient robustness against disturbances and uncertainties. In these cases, disturbances are not explicitly modelled or estimated but are tolerated through controller tuning and feedback corrections.

The authors in [22] proposed a generalized predictive control strategy for an elastic actuator-driven exoskeleton robot. While robustness is not incorporated explicitly into the predictive formulation through uncertainty or disturbance modelling, it is evaluated experimentally by injecting artificial uncertainties, relying on the receding-horizon correction to compensate modelling errors. In [23], an MPC scheme for trajectory tracking of an unmanned aerial vehicle was presented, where external disturbances are not included in the predictive formulation. A Kalman filter is used only for state and reference estimation of a ground vehicle. In this case, uncertainty is handled in the estimation stage, whereas the MPC is formulated without considering disturbances.

By its part, the proposed MPC in [24] operates based on the nominal dynamics of a wind turbine system and relies entirely on state estimates provided by a terminal sliding mode observer. Nevertheless, the observer is not designed to estimate external disturbances, but rather to ensure reliable state reconstruction in the presence of sensor faults. A superheater of a thermal power plant was controlled using MPC in [25]. Disturbances, such as load variations and operating point changes, are not explicitly modelled or estimated, but handled implicitly through the receding-horizon feedback of the MPC and robust parameter tuning, optimized offline using an improved fruit fly algorithm.

In the previous works, controllers rely on the iterative solution of the optimization problem at each sampling instant, which corrects the effect of unmodelled disturbances through state feedback. In contrast, our proposal incorporates disturbance dynamics directly into the predictive formulation, so robustness arises from the model structure itself rather than only from constant correction.

In contrast to conventional MPC-based strategies, the proposed framework requires only velocity measurements, avoiding full-state feedback or auxiliary observer design. This is enabled by the integration of differential flatness and polynomial disturbance modelling, which embeds both state reconstruction and disturbance dynamics directly within the predictive control formulation.

Additionally, some works address model uncertainty and external disturbances by reformulating the system model. In this way, undesired effects are handled implicitly through model adaptation rather than explicit estimation. In [26], a linear parameter-varying MPC–LQR scheme was designed for active suspension control. In this approach, nonlinearities and external road excitations are embedded into the model through scheduling parameters. The controller is thus able to adapt to varying operating conditions while disturbance effects are implicitly managed via parameter variations. In comparison, our approach preserves the disturbance as an explicit dynamic component and incorporates its temporal evolution directly into the predictive model along the prediction horizon.

Another theoretical aspect relevant to this work is differential flatness. Differential flatness is a structural property present in a wide variety of controllable systems and allows the simplification of both trajectory planning and control synthesis since it eliminates the need to solve complex differential equations offering a complete system parametrization including state, input and output variables through a set of independent variables known as flat outputs and their derivatives [27]. Its application not only facilitates controller formulation, but also significantly improves the ability of the system to follow desired trajectories with precision.

For DC motor control, classical techniques may be limited and degraded by physical constraints or external disturbances. In this context, differential flatness arises as an efficient alternative for modelling and controlling such systems, since all motor states and control inputs can be expressed as functions of a flat output and its derivatives. This property facilitates the design of structured control strategies, such as MPC, enabling the explicit inclusion of constraints on system variables as well as a proper handling of uncertainty and disturbances.

By merging both techniques, the control problem can be transformed into an optimized and solvable real-time formulation. Reported works have successfully applied this integration to complex systems from different perspectives, such as mobile manipulators [28] and aerial vehicles [29], aiming its applicability and adaptation to electromechanical systems such as DC-motors coupled gearhead systems.

While differential flatness-based MPC has been successfully applied to nonlinear systems [30], reported approaches typically assume that external disturbances are either known a priori or treated as exogenous signals, without explicit estimation or dynamic compensation within the predictive controller. Conversely, in the work reported in [31], a multi-variable fixed-time disturbance observer-based model predictive control algorithm is proposed for trajectory tracking of disturbed quadrotors, where differential flatness is exploited only for reference trajectory generation, rather than for the formulation of the predictive control model. During the MPC optimization, the estimated disturbance is assumed to remain constant, enabling robust compensation against bounded external effects.

In contrast with reported works, this paper proposes an advanced speed control framework for disturbed DC motor–gearhead drive systems, in which a suitable integration of model predictive control, the structural property of differential flatness and a Kalman filter scheme are systematically exploited. The combination of these methodologies improves trajectory tracking and the robustness of the system against external load torque disturbances and noisy measurements of the controlled output. Furthermore, the effects of measurement noise are explicitly evaluated, an aspect that is often neglected in most MPC-based studies reported in the literature.

The main contributions of this paper are summarized as follows:

1. An improved MPC framework based on a differential flatness system model.
2. A polynomial Kalman filter design for dynamic load torque estimation based on a flatness formulation.
3. An augmented flat model that incorporates dynamic disturbance compensation within the MPC framework.

The remainder of the paper is organized as follows: Section 2 presents the theoretical foundations and the mathematical modelling of the electromechanical system as well as the full parametrization from a differential flatness perspective; Section 3 gives an overview of the MPC control technique while Section 4 details the MPC framework design using the flat system model and a suitably integration of the Kalman-based polynomial estimator; Section 5 provides main computational results and a meticulous and comprehensive comparison against other effective control schemes. Finally, Section 6 concludes the paper with key findings and future research directions.

2. Mathematical Modelling of the System

The DC motor–gearhead drive is a differentially flat dynamical system with the gearhead shaft speed working as the flat output, where the state and control variables can be expressed as functions of the flat output and a finite number of its time derivatives [32]. The system converts electrical energy into mechanical energy and consists of a DC electric motor coupled to a gearhead assembly, as shown in Figure 1. This system is commonly employed to provide mayor mechanical power which is highly demanded in diverse engineering applications.

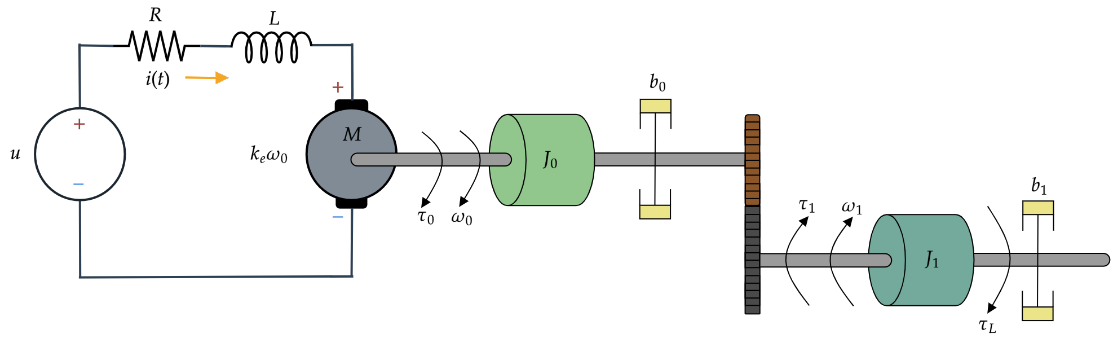

Figure 1. Main electromechanical schematic diagram of the DC motor–gearhead drive system.

The electrical subsystem is integrated by the passive elements R and L standing for the motor's armature resistance and inductance, respectively. The input voltage variable is denoted by u and the armature current is denoted by i. The back emf voltage is expressed in terms of the motor angular speed as $e_F = k_e\omega_0$, meantime the electric torque produced by the motor shaft is given as a function of the armature current as $\tau_0 = k_m i$, where k_e and k_m are the electric and torque constants which allows the energy transformation.

The mechanical subsystem is compounded by a speed reducer coupled to the motor shaft to reduce the angular velocity through a reduction ratio η, while simultaneously increasing the torque available on the output shaft. The motor and the reducer are characterized by their respective inertia and viscous friction coefficients. Specifically, J_0 and b_0 denote the motor inertia and viscous friction, whereas J_1 and b_1 represent the corresponding parameters of the reducer [33].

Newton and Kirchhoff laws are used to derive the dynamic model of the system, containing the equations of the motor and the speed reducer, which are divided into the mechanical and electrical parts:

$$\begin{aligned}\left(J_1 + \eta^2 J_0\right)\dot{\omega}_1 &= -\left(b_1 + \eta^2 b_0\right)\omega_1 + \eta k_m i - \tau_L \\ L\frac{di}{dt} &= -Ri - \eta k_e \omega_1 + u.\end{aligned} \tag{1}$$

To simplify the notation, the equivalent inertia and damping terms are defined as $J_e = J_1 + \eta^2 J_0$ and $b_e = b_1 + \eta^2 b_0$. Substituting these expressions into (1) yields the simplified form in (2).

$$\begin{aligned}J_e\dot{\omega}_1 &= -b_e\omega_1 + \eta k_m i - \tau_L \\ L\frac{di}{dt} &= -Ri - \eta k_e \omega_1 + u,\end{aligned} \tag{2}$$

Therefore, the state-space representation in (3) is obtained by defining the state variables as $z_{e_1} = \omega_1$ and $z_{e_2} = i$, and rewriting the system in first-order form:

$$\begin{aligned}\dot{\mathbf{z}}_e(t) &= \mathbf{A}_{e_c}\,\mathbf{z}_e(t) + \mathbf{B}_{e_c}\,u(t) + \mathbf{E}_{e_c}\,\tau_L(t), \\ y_e(t) &= \mathbf{C}_{e_c}\,\mathbf{z}_e(t),\end{aligned} \tag{3}$$

where

$$\mathbf{A}_{e_c} = \begin{bmatrix} -\frac{b_e}{J_e} & \frac{nk_m}{J_e} \\ -\frac{nk_e}{L} & -\frac{R}{L} \end{bmatrix}, \qquad \mathbf{B}_{e_c} = \begin{bmatrix} 0 \\ \frac{1}{L} \end{bmatrix}, \tag{4}$$

$$\mathbf{E}_{e_c} = \begin{bmatrix} -\frac{1}{J_e} \\ 0 \end{bmatrix}, \qquad \mathbf{C}_{e_c} = \begin{bmatrix} 1 & 0 \end{bmatrix}. \tag{5}$$

Remark 1. *Throughout this work, the state vector $\mathbf{z}(\cdot)$ is used to denote continuous-time system representations, while discrete-time models are expressed in terms of $\mathbf{x}(\cdot)$.*

2.1. Flat Model of the DC Motor–Gearhead Drive System

The electromechanical system represented by the equations in (2) is differentially flat, and can be parametrized with flat output given by the angular velocity of the gearhead output shaft, $y_f = \omega_1$. Thus, for purposes of proper speed tracking control design the system can be analysed considering the disturbing load torque term and the following time derivatives:

$$\dot{y}_f = -\frac{b_e}{J_e}\omega_1 + \frac{\eta k_m}{J_e} i - \frac{1}{J_e}\tau_L. \tag{6}$$

For the second derivative, the equation (6) will be derived with respect to time:

$$\ddot{y}_f = \frac{d}{dt}\left(-\frac{b_e}{J_e}\omega_1 + \frac{\eta k_m}{J_e} i - \frac{1}{J_e}\tau_L\right) \tag{7}$$

thus,

$$\ddot{y}_f = -\frac{b_e}{J_e}\dot{\omega}_1 + \frac{\eta k_m}{J_e}\frac{di}{dt} - \frac{1}{J_e}\dot{\tau}_L. \tag{8}$$

Note that the derivative of armature current is already known from (2) as

$$\frac{di}{dt} = -\frac{R}{L}i - \frac{\eta k_e}{L}\omega_1 + \frac{1}{L}u \tag{9}$$

and by substituting this expression into the Equation (8) we have

$$\ddot{y}_f = -\frac{b_e}{J_e}\dot{\omega}_1 + \frac{\eta k_m}{J_e}\left(-\frac{R}{L}i - \frac{n k_e}{L}\omega_1 + \frac{1}{L}u\right) - \frac{1}{J_e}\dot{\tau}_L. \tag{10}$$

Then, by solving the multiplication we have

$$\ddot{y}_f = -\frac{b_e}{J_e}\dot{\omega}_1 - \frac{\eta k_m R}{J_e L}i - \frac{\eta^2 k_e k_m}{J_e L}\omega_1 + \frac{\eta k_m}{J_e L}u - \frac{1}{J_e}\dot{\tau}_L. \tag{11}$$

From the above equations, the current and voltage variables can be expressed in terms of the flat output y_f, its derivatives $\dot{y}_f, \ddot{y}_f$, and the disturbance load torque τ_L. Thus, the current is cleared from the equation in (6) as follows:

$$i = \frac{J_e}{\eta k_m}\dot{y}_f + \frac{b_e}{\eta k_m}y_f + \frac{1}{k_m}\tau_L. \tag{12}$$

The disturbance term τ_L represents a lumped external load torque acting on the motor shaft, accounting for variations due to mechanical loading, transmission effects, and unmodeled dynamics.

Next, the explicit expression for u is derived from Equation (11):

$$u = \frac{J_e L}{\eta k_m}\left(\ddot{y}_f + \frac{b_e}{J_e}\dot{y}_f + \frac{\eta k_m R}{J_e L}i + \frac{\eta^2 k_e k_m}{J_e L}y_f + \frac{1}{J_e}\dot{\tau}_L\right), \tag{13}$$

and by substituting (12) into (13), the following expression is obtained

$$u = \frac{J_e L}{\eta k_m}\left[\ddot{y}_f + \left(\frac{b_e}{J_e} + \frac{R}{L}\right)\dot{y}_f + \left(\frac{\eta^2 k_e k_m + R b_e}{J_e L}\right)y_f + \frac{R}{J_e L}\tau_L + \frac{1}{J_e}\dot{\tau}_L\right]. \tag{14}$$

Finally, substituting these expressions into the equation for $\ddot{y}_f$, we obtain the perturbed input–output form:

$$\ddot{y}_f + a_1\dot{y}_f + a_0 y_f = bu - \frac{R}{J_e L}\tau_L - \frac{1}{J_e}\dot{\tau}_L. \tag{15}$$

Considering a generalized disturbance term in (15), the equation can be rewritten as

$$\ddot{y}_f + a_1\dot{y}_f + a_0 y_f = bu + \xi, \tag{16}$$

with

$$\xi = -\frac{R}{J_e L}\tau_L - \frac{1}{J_e}\dot{\tau}_L \tag{17}$$

where the coefficients are defined as

$$\begin{aligned} a_0 &= \frac{\eta^2 k_m k_e + R b_e}{J_e L} \\ a_1 &= \frac{b_e}{J_e} + \frac{R}{L} \\ b &= \frac{\eta k_m}{J_e L}. \end{aligned} \tag{18}$$

The coefficients a_0, a_1, and b depend on the physical parameters of the system, such as inertia, damping, and motor constants, and capture the dynamic behaviour of the electromechanical system. Additionally, the term ξ explicitly reveals the influence of the load torque disturbance and its time derivative on the control input.

Flat State-Space Model

Considering the second-order dynamic model given in (16), and the state variables as $z_{f_1} = y_f$ and $z_{f_2} = \dot{y}_f$, the system can be rewritten as the set of first-order differential equations below

$$\begin{aligned} \dot{z}_{f_1} &= z_{f_2} \\ \dot{z}_{f_2} &= -a_0 z_{f_1} - a_1 z_{f_2} + bu + \xi. \end{aligned} \tag{19}$$

Therefore, the flat continuous state-space representation is given as follows,

$$\begin{aligned} \dot{\mathbf{z}}_f(t) &= \mathbf{A}_{f_c}\, \mathbf{z}_f(t) + \mathbf{B}_{f_c}\, u(t) + \mathbf{E}_{f_c}\, \xi(t), \\ y_f(t) &= \mathbf{C}_{f_c}\, \mathbf{z}_f(t), \end{aligned} \tag{20}$$

with

$$\mathbf{A}_{f_c} = \begin{bmatrix} 0 & 1 \\ -a_0 & -a_1 \end{bmatrix}, \quad \mathbf{B}_{f_c} = \begin{bmatrix} 0 \\ b \end{bmatrix}, \quad \mathbf{C}_{f_c} = \begin{bmatrix} 1 & 0 \end{bmatrix}, \quad \mathbf{E}_{f_c} = \begin{bmatrix} 0 \\ 1 \end{bmatrix}.$$

This flat model will be used for MPC design purposes in subsequent sections.

3. Model Predictive Control Design

Model Predictive Control enables the prediction of a system's future behaviour over a finite prediction horizon by solving, at each sampling instant, an optimization problem that computes an optimal sequence of manipulated variables [6,34]. This is achieved using a mathematical model of the plant, which may be linear or nonlinear, with the objective of optimizing a given performance criterion while accounting for disturbances and uncertainties [35,36]. MPC is built upon four fundamental pillars; the system model, state estimation, prediction, and optimization.

At each decision instant k, the current state of the system is estimated and used to predict its future evolution over a finite horizon. A sequence of control actions is computed by minimizing a cost function, but only the first element of the optimal sequence, referred to as the optimal control action, is applied during the interval $[k, k+1]$. This receding-horizon procedure is repeated at every sampling instant, and its straightforward computational structure also makes MPC well suited for implementation on microprocessors [11,37]. In this work, MPC is integrated with differential flatness and Kalman filtering to form a composite control framework for accurate output tracking of a disturbed DC motor–gearhead drive system.

3.1. Prediction Horizon

The system dynamics are described in discrete time by the next general model

$$\mathbf{x}(k+1) = \mathbf{f}\big[\mathbf{x}(k), \mathbf{u}(k)\big], \tag{21}$$

where $\mathbf{x}(k) \in \mathbb{R}^{n}$ is the state vector, and $\mathbf{u}(k) \in \mathbb{R}^{n_u}$ is the control input vector with n_u inputs. To predict the system behaviour over a finite horizon of length N, the predicted state trajectory is defined as

$$\tilde{\mathbf{x}}(k) = \begin{bmatrix} \mathbf{x}(k+1) \\ \mathbf{x}(k+2) \\ \vdots \\ \mathbf{x}(k+N) \end{bmatrix} \in \mathbb{R}^{nN}, \tag{22}$$

while the corresponding future control input sequence is given by

$$\tilde{\mathbf{u}}(k) = \begin{bmatrix} \mathbf{u}(k) \\ \mathbf{u}(k+1) \\ \vdots \\ \mathbf{u}(k+N-1) \end{bmatrix} \in \mathbb{R}^{n_u N}. \tag{23}$$

The predicted state trajectory is determined by the current state $\mathbf{x}(k)$, the future control sequence $\tilde{\mathbf{u}}(k)$, the sampling period T_s, and the prediction horizon N. This dependency can be expressed as

$$\tilde{\mathbf{x}}(k \mid \tilde{\mathbf{u}}) = \mathcal{F}\big[\mathbf{x}(k), \tilde{\mathbf{u}}(k), T_s, N\big], \tag{24}$$

where $\mathcal{F}(\cdot)$ denotes the state transition mapping induced by the system dynamics.

3.2. Discrete-Time Model

For MPC implementation, the system to be controlled is represented in discrete time under a zero-order hold assumption. The discrete-time state-space model is given by

$$\begin{aligned} \mathbf{x}(k+1) &= \mathbf{A}_d\mathbf{x}(k) + \mathbf{B}_d\mathbf{u}(k), \\ \mathbf{y}(k) &= \mathbf{C}_d\mathbf{x}(k), \end{aligned} \tag{25}$$

where $\mathbf{y}(k) \in \mathbb{R}^{n_r}$ is the output vector and the discrete-time matrices are obtained via exact discretization as

$$\begin{aligned} \mathbf{A}_d &= e^{\mathbf{A}_c T_s}, \\ \mathbf{B}_d &= \int_0^{T_s} e^{\mathbf{A}_c \tau}\mathbf{B}_c \, d\tau, \end{aligned} \tag{26}$$

where $\mathbf{A}_c$ and $\mathbf{B}_c$ are the continuous state and control matrices.

3.3. State Prediction Model

The predicted state at step $(k+i)$ can be written as

$$\mathbf{x}(k+i) = \mathbf{\Phi}_i\mathbf{x}(k) + \mathbf{\Psi}_i\tilde{\mathbf{u}}(k), \quad i = 1, \ldots, N, \tag{27}$$

where $\mathbf{\Phi}_i \in \mathbb{R}^{n\times n}$ and $\mathbf{\Psi}_i \in \mathbb{R}^{n\times n_u N}$ are prediction matrices derived from $\mathbf{A}_d$ and $\mathbf{B}_d$.

3.4. Proposed Cost Function

To find the best sequence of control action, in the present work, the value of the cost function $J(u|x(k), y^{\star}(k), u^{\star})$ is defined over the prediction horizon $[k, k+N]$ as follows [38]:

$$J_{\text{MPC}} := \sum_{i=1}^{N} \|\mathbf{y}(k+i) - \mathbf{y}^{\star}(k+i)\|^2_{\mathbf{Q}_y} + \sum_{i=1}^{N} \|\mathbf{u}(k+i-1) - \mathbf{u}^{\star}\|^2_{\mathbf{Q}_u}, \tag{28}$$

where $\mathbf{Q}_y \in \mathbb{R}^{n_y \times n_y}$ is a positive semi-definite weighting matrix that penalizes the output tracking error, and $\mathbf{Q}_u \in \mathbb{R}^{n_u \times n_u}$ is a positive definite weighting matrix that penalizes variations in the control input.

Using the predicted state and input trajectories, the MPC cost function in (28) can be rewritten in the standard quadratic form of a constrained optimization problem. In the general case, when non-zero reference trajectories are considered, the compact formulation is given by

$$J_{\text{MPC}} = \frac{1}{2}\tilde{\mathbf{u}}^{\top}\mathbf{H}\tilde{\mathbf{u}} + [\mathbf{F}\mathbf{x}(k) - \mathbf{F}_r\mathbf{r}]\tilde{\mathbf{u}} + \gamma, \tag{29}$$

where $\mathbf{r}$ denotes the stacked reference trajectory over the prediction horizon, constructed from the desired output values $\mathbf{y}^{\star}(k+i)$, $i = 1, \ldots, N$. Thus, $\mathbf{r}$ represents a compact vector form of the same desired output trajectory used in the expanded cost function.

Note that the constant term γ arises from the expansion of the quadratic cost function. For instance, when expanding the output tracking term

$$\|\mathbf{y}(k+i) - \mathbf{y}^{\star}(k+i)\|^2_{\mathbf{Q}_y},$$

independent terms appear but do not multiply the optimization variable $\tilde{\mathbf{u}}$ and therefore do not influence the minimization process.

$$\tilde{\mathbf{u}}^{\text{opt}} = -\mathbf{H}^{-1}\mathbf{F}\mathbf{x}(k) + \mathbf{H}^{-1}\mathbf{F}_r\mathbf{r}. \tag{30}$$

Conversely, the regulation problem is recovered as a particular case by setting $\mathbf{y}^{\star} = \mathbf{0}$ and $\mathbf{u}^{\star} = \mathbf{0}$, which yields the simplified cost function

$$J_{\text{MPC}} = \frac{1}{2}\tilde{\mathbf{u}}^{\top}\mathbf{H}\tilde{\mathbf{u}} + \mathbf{F}\mathbf{x}(k)\tilde{\mathbf{u}}. \tag{31}$$

The optimal control sequence is thus given by

$$\tilde{\mathbf{u}}^{\text{opt}}[\mathbf{x}(k)] = -\mathbf{H}^{-1}\mathbf{F}\mathbf{x}(k), \tag{32}$$

In both situations, $\mathbf{H}$ and $\mathbf{F}$ are obtained from the prediction and weighting matrices, where the control action applied to the system is the first element of $\tilde{\mathbf{u}}^{\text{opt}}$.

4. Model Predictive Control Design and Flatness-Based Extension

This section introduces the design and evaluation of different control schemes to highlight the performance of the proposed MPC framework. A linear quadratic integral (LQI) controller, a feed-forward PID-like controller and an offset-free MPC with disturbance-state augmentation are properly proposed for speed output tracking control tasks.

4.1. Linear Quadratic Integral Control Design

The LQI controller is based on optimal state-feedback with integral action. First, consider the disturbed nominal equivalent model introduced in (3) which can be straightforward derived into the following discrete state-space model:

$$\begin{aligned}\mathbf{x}_e(k+1) &= \mathbf{A}_{e_d}\mathbf{x}_e(k) + \mathbf{B}_{e_d}u(k) + \mathbf{E}_{e_d}\tau_L(k),\\ y_e(k) &= \mathbf{C}_{e_d}\mathbf{x}_e(k),\end{aligned} \tag{33}$$

where the discrete-time state and input matrices are obtained as

$$\begin{aligned}\mathbf{A}_{e_d} &= e^{\mathbf{A}_{e_c}T_s},\\ \mathbf{B}_{e_d} &= \int_0^{T_s} e^{\mathbf{A}_{e_c}\tau}\mathbf{B}_{e_c}\,d\tau,\\ \mathbf{E}_{e_d} &= \int_0^{T_s} e^{\mathbf{A}_{e_c}\tau}\,\mathbf{E}_{e_c}\,d\tau.\end{aligned} \tag{34}$$

Here, $\mathbf{A}_{e_c}$ and $\mathbf{B}_{e_c}$ are the continuous-time state and control matrices from continuous model (3); $\tau_L(k)$ represents the unknown load torque disturbance; and $\mathbf{x}_e(k) \in \mathbb{R}^2$ is the state vector at time k, defined as

$$\mathbf{x}_e(k) = \begin{bmatrix}\omega_1(k)\\ i(k)\end{bmatrix}, \tag{35}$$

where $\omega_1(k)$ denotes the gearhead shaft output angular speed and represents the controlled output $y_e(k) \in \mathbb{R}$; $i(k)$ is the armature current; and $u(k) \in \mathbb{R}$ denotes the scalar control input at time k. To enforce zero steady-state error, the following integral augmented state is defined based on the output tracking error:

$$e_e(k) = y_e^\star(k) - y_e(k), \tag{36}$$

$$x_I(k+1) = x_I(k) + T_s\,e_e(k). \tag{37}$$

The augmented state vector is defined as

$$\mathbf{x}_{e_a}(k) = \begin{bmatrix}\mathbf{x}_e(k)\\ x_I(k)\end{bmatrix} \in \mathbb{R}^3, \tag{38}$$

and the resulting discrete-time augmented model is given by

$$\begin{aligned}\mathbf{x}_{e_a}(k+1) &= \mathbf{A}_{e_a}\,\mathbf{x}_{e_a}(k) + \mathbf{B}_{e_a}\,u(k) + \mathbf{E}_{e_a}\,\tau_L(k) + \mathbf{B}_{\mathrm{r}}\,y_e^\star(k),\\ y_e(k) &= \mathbf{C}_{e_a}\,\mathbf{x}_{e_a}(k),\end{aligned} \tag{39}$$

with

$$\mathbf{A}_{e_a} = \begin{bmatrix}\mathbf{A}_{e_d} & \mathbf{0}_{2\times1}\\ -T_s\mathbf{C}_{e_d} & 1\end{bmatrix}, \qquad \mathbf{B}_{e_a} = \begin{bmatrix}\mathbf{B}_{e_d}\\ 0\end{bmatrix}, \qquad \mathbf{E}_{e_a} = \begin{bmatrix}\mathbf{E}_{e_d}\\ 0\end{bmatrix}, \tag{40}$$

$$\mathbf{B}_r = \begin{bmatrix}\mathbf{0}_{2\times1}\\ T_s\end{bmatrix}, \quad \text{and} \quad \mathbf{C}_{e_a} = \begin{bmatrix}\mathbf{C}_{e_d} & 0\end{bmatrix}. \tag{41}$$

The LQI control law is then obtained by minimizing the infinite-horizon quadratic performance index related to the following quadratic cost function,

$$J_{\text{LQI}} := \sum_{k=0}^{\infty} \Big[\mathbf{x}_{e_a}(k)^{\top} \mathbf{Q}\, \mathbf{x}_{e_a}(k) + R_u\, u(k)^2 \Big], \tag{42}$$

where $\mathbf{Q} \in \mathbb{R}^{3\times 3} \succeq 0$ is a symmetric weighting matrix and $R_u \in \mathbb{R}$, $R_u > 0$ is a scalar weight. $\mathbf{Q}$ penalizes the augmented state $\mathbf{x}_{e_a}(k)$, including the physical states and the integral state $x_I(k)$ associated with the tracking error, whereas R_u penalizes the control effort $u(k)$.

In this fashion, the optimal discrete-time LQI feedback gain $\mathbf{K}_{\text{LQI}}$ is computed from the solution of the discrete algebraic Riccati equation associated with (39) and (42). Therefore, the resulting control law is given by

$$u(k) = -\mathbf{K}_{\text{LQI}}\, \mathbf{x}_{e_a}(k), \tag{43}$$

with

$$\mathbf{K}_{\text{LQI}} = \Big[\mathbf{K}_{x_e} \quad k_I \Big], \tag{44}$$

where $\mathbf{K}_{x_e} \in \mathbb{R}^{1\times 2}$ is the state-feedback gain and $k_I \in \mathbb{R}$ is the integral gain. By substituting the defined augmented state into the control law, the implemented discrete control input can be written explicitly as

$$u(k) = -\mathbf{K}_{x_e}\, \mathbf{x}_e(k) - k_I\, x_I(k). \tag{45}$$

Since the LQI controller is designed in discrete time, the integral augmentation (37) explicitly depends on the sampling time T_s. In the numerical evaluation of this work, two sampling times are considered: $T_s = 1$ ms and $T_s = 10$ ms. In subsequent sections, the performance of the LQI controller is reported under constant and time-varying load torque disturbances, using the same reference profile and disturbance signals employed for the MPC-based controllers.

4.2. Feed-Forward Proportional-Integral-Derivative Control

In motor control applications, with in mechanical process automation, PID controllers have been extensively [39]. In this fashion, a baseline controller consisting of a PID with model-based feed-forward is implemented for comparison purposes. The controller is designed based on the flat representation of the DC motor–gearhead in (16). The feed-forward term is obtained by neglecting ξ and imposing perfect tracking as follows:

$$\lim_{t\to\infty} \big(y_f - y_f^{\star}\big) = 0, \qquad \lim_{t\to\infty} \big(\dot{y}_f - \dot{y}_f^{\star}\big) = 0, \qquad \lim_{t\to\infty} \big(\ddot{y}_f - \ddot{y}_f^{\star}\big) = 0. \tag{46}$$

Thus, substituting these relations into the second-order flat model introduced in (16) we have,

$$\ddot{y}_f^{\star} + a_1 \dot{y}_f^{\star} + a_0 y_f^{\star} = b u_f^{\star}, \tag{47}$$

and the resulting feed-forward input term is proposed as follows:

$$u_f^{\star} = \frac{1}{b}\Big(\ddot{y}_f^{\star} + a_1 \dot{y}_f^{\star} + a_0 y_f^{\star} \Big). \tag{48}$$

To ensure consistency with the discrete-time framework adopted throughout this work employing sampling period T_s, the feed-forward term (48) is implemented in discrete time. Note that the reference derivatives can alternatively be approximated via forward finite differences as

$$\dot{y}_f^\star(kT_s) \approx \frac{y_f^\star(k+1) - y_f^\star(k)}{T_s}, \tag{49}$$

$$\ddot{y}_f^\star(kT_s) \approx \frac{y_f^\star(k+2) - 2y_f^\star(k+1) + y_f^\star(k)}{T_s^2}. \tag{50}$$

The above forward-difference approximation is formulated since the reference trajectory is assumed to be known *a priori* over the future horizon. By substituting above equations into (48) yields the discrete-time feed-forward term

$$u_f^\star(k) = \frac{1}{b}\left[\frac{y_f^\star(k+2) - 2y_f^\star(k+1) + y_f^\star(k)}{T_s^2} + a_1\frac{y_f^\star(k+1) - y_f^\star(k)}{T_s} + a_0 y_f^\star(k)\right].$$

To provide robustness against load torque disturbances and modelling uncertainties, a feedback term is also integrated with the tracking error defined as

$$e(k) = y_f^\star(k) - y_f(k). \tag{51}$$

Then, the next discretized PID is implemented in incremental form as follows:

$$\Delta u_{\text{PID}}(k) = K_p[e(k) - e(k-1)] + K_i T_s\, e(k) + \frac{K_d}{T_s}[e(k) - 2e(k-1) + e(k-2)],$$

and

$$u_{\text{PID}}(k) = u_{\text{PID}}(k-1) + \Delta u_{\text{PID}}(k), \tag{52}$$

where K_p, K_i, and K_d denote the proportional, integral, and derivative gains, respectively. In this fashion, the feed-forward term exploits the availability of the planned reference trajectory and the feedback term is implemented using measured output data. Thus, the control input is given by the sum of the feed-forward and feedback terms as

$$u(k) = u_f^\star(k) + u_{\text{PID}}(k), \tag{53}$$

subject to the input saturation constraint

$$u_{\min} \leq u(k) \leq u_{\max}. \tag{54}$$

Remark 2. *Although the plant model is discretized under a zero-order hold assumption, the feed-forward term is computed from the sampled reference trajectory using forward finite-difference approximations of its time derivatives. Both the plant model and the feed-forward computation share the same sampling period T_s, ensuring consistency within the discrete-time design.*

4.3. Offset-Free MPC via Disturbance-State Augmentation

Although the control formulations presented in the previous subsections ensures optimal tracking performance under nominal conditions, steady-state offsets may arise in the presence of disturbances or model uncertainty. To address this issue, an offset-free MPC based on disturbance-state augmentation is proposed.

Offset-free tracking in MPC has been extensively studied through the augmentation of the plant dynamical model with disturbance states, combined with observer-based schemes for simultaneous state and disturbance estimation. Such approaches have demonstrate adequately offset-free reference tracking under constant or slowly varying disturbances within the MPC design [14,16,19,40]. However, there is no evidence of previous proposals employing flat models for output tracking control of DC motor–gearhead drive systems, so the MPC design presented in the previous section is now reformulated for offset-free tracking.

From the equations in (20), let the discrete-time flat model be described by

$$\begin{aligned} \mathbf{x}_f(k+1) &= \mathbf{A}_{f_d}\mathbf{x}_f(k) + \mathbf{B}_{f_d}u(k) + \mathbf{E}_{f_d}\xi(k), \\ y_f(k) &= \mathbf{C}_{f_d}\mathbf{x}_f(k), \end{aligned} \tag{55}$$

where $\mathbf{x}_f(k) \in \mathbb{R}^{n_f}$ denotes the discrete flat-state vector and $\xi(k) \in \mathbb{R}^{n_d}$ represents an unknown constant or slowly varying disturbance load torque acting on the system. Moreover, the system output $y_f(k) \in \mathbb{R}$ is scalar and corresponds to the flat output. The matrices of this model are obtained in a similar manner by applying the exact discretization formulas in (26).

To enable offset-free tracking, the disturbance is modelled as an integrator

$$\xi(k+1) = \xi(k). \tag{56}$$

Based on (55) and (56), the proposed augmented flat-state vector employed within the MPC design is defined as

$$\mathbf{x}_{f_a}(k) = \begin{bmatrix} \mathbf{x}_f(k) \\ \xi(k) \end{bmatrix} \in \mathbb{R}^{n_\mathrm{f}+n_d}. \tag{57}$$

Therefore the resulting augmented flat-state model is then given as

$$\begin{aligned} \mathbf{x}_{f_a}(k+1) &= \underbrace{\begin{bmatrix} \mathbf{A}_{f_d} & \mathbf{E}_{f_d} \\ \mathbf{0} & \mathbf{I} \end{bmatrix}}_{\mathbf{A}_{fa}} \mathbf{x}_{f_a}(k) + \underbrace{\begin{bmatrix} \mathbf{B}_{f_d} \\ \mathbf{0} \end{bmatrix}}_{\mathbf{B}_{fa}} u(k), \\ y_f(k) &= \underbrace{\begin{bmatrix} \mathbf{C}_f & \mathbf{0} \end{bmatrix}}_{\mathbf{C}_{fa}} \mathbf{x}_{f_a}(k). \end{aligned} \tag{58}$$

Thus, based on (27) the augmented flat-state representation is given as follows:

$$\mathbf{x}_{f_a}(k+i) = \mathbf{\Phi}_{f_a,i}\mathbf{x}_{f_a}(k) + \mathbf{\Psi}_{f_a,i}\tilde{\mathbf{u}}(k), \quad i = 1, \ldots, N, \tag{59}$$

with the predicted output computed as

$$y_f(k+i) = \mathbf{C}_{f_a}\mathbf{x}_{f_a}(k+i). \tag{60}$$

The quadratic cost function defined in (28) remains unchanged, ensuring offset-free tracking through internal disturbance estimation embedded in the augmented flat-state vector $\mathbf{x}_{f_a}(k)$, without introducing explicit integral action. Since the augmented disturbance state $\xi(k)$ is unknown and not directly measurable, an augmented-state Kalman filter is employed to estimate the flat-state vector and the disturbance term. The estimator is designed based on the augmented model in (58), assuming additive process and measurement noise.

The augmented system is described as

$$\begin{aligned} \mathbf{x}_{f_a}(k+1) &= \mathbf{A}_{f_a}\mathbf{x}_{f_a}(k) + \mathbf{B}_{f_a}u(k) + \mathbf{w}(k), \\ y_f(k) &= \mathbf{C}_{f_a}x_{f_a}(k) + v(k), \end{aligned} \tag{61}$$

where $\mathbf{w}(k)$ and $v(k)$ denote zero-mean white Gaussian process and measurement noise with covariance matrices Q and R, respectively.

The Kalman filter recursively computes the minimum-variance estimate $\hat{\mathbf{x}}_{f_a}(k)$ of the augmented state, including the disturbance component $\hat{\xi}(k)$, which is then directly used by the MPC prediction model to compensate steady-state offsets caused by unknown load torque disturbances.

4.4. MPC Framework with Kalman Filtering–Polynomial Torque Estimation

This section presents an enhanced MPC framework capable of handling variable load torque disturbances by combining polynomial disturbance modelling with Kalman filtering, representing the core contribution of this work. The proposed framework extends the disturbance-state augmentation strategy introduced in Section 4.3, relaxing the assumption of constant or slowly varying load torque disturbances acting on the DC motor–gearhead drive system.

In the nominal offset-free MPC formulation, the disturbance was represented by a constant or considerably slowly varying term modelled as an integrator. While this assumption is sufficient to eliminate steady-state offsets, real load torques may exhibit frequency variations as well as stochastic effects. To capture these characteristics, the generalized disturbance acting on the system is assumed to be dynamic and containing unmodelled dynamics.

4.4.1. Polynomial Disturbance Representation

The disturbance signal is proposed to be approximated by a finite-order polynomial model, which generalizes the integrator-based assumption employed in classical offset-free MPC. The model provides a structured representation of the generalized load torque disturbance as a finite-order sum of incremental components over a small time window. Rather than estimating a static disturbance term, the proposed approach captures its dynamic behaviour through a chain of discrete-time integrators.

For a polynomial model of order p, the disturbance-state vector is defined as

$$\mathbf{d}(k) = \begin{bmatrix} d_0(k) & d_1(k) & \cdots & d_p(k) \end{bmatrix}^\top \in \mathbb{R}^{n_p}, \qquad n_p = p+1, \tag{62}$$

where $d_0(k)$ represents the instantaneous value of the generalized disturbance, while the higher-order states account for its successive discrete-time increments. The corresponding disturbance dynamics can be expressed as

$$\begin{aligned} d_0(k+1) &= d_0(k) + d_1(k), \\ d_1(k+1) &= d_1(k) + d_2(k), \\ &\vdots \\ d_{p-1}(k+1) &= d_{p-1}(k) + d_p(k), \\ d_p(k+1) &= d_p(k), \end{aligned} \tag{63}$$

which corresponds to a chain of integrators generating a polynomial disturbance profile. This formulation generalizes the classical integrator-based offset-free assumption with order $p = 0$ and enables the representation of constant, ramp-like, and higher-order varying torque disturbances.

Equivalently, (63) can be compactly written as

$$\mathbf{d}(k+1) = \mathbf{\Gamma}_{\xi}\, \mathbf{d}(k), \tag{64}$$

where $\mathbf{\Gamma}_\xi \in \mathbb{R}^{n_p \times n_p}$ is the polynomial matrix associated with the selected order p. A polynomial-order $p = 4$ is adopted in this work.

Within the proposed architecture, the disturbance state vector $\mathbf{d}(k)$ is included in the augmented state and estimated online by a Kalman filter, where the generalized disturbance acting on the system is reconstructed from $\hat{\xi}(k) = \hat{d}_0(k|k)$.

4.4.2. Augmented Prediction Model

Based on the polynomial disturbance representation above, the flat state vector used for prediction and control is augmented to explicitly include the disturbance-related states. The new augmented flat state vector is defined as

$$\mathbf{x}_{f_A}(k) = \begin{bmatrix} \mathbf{x}_f(k) \\ \mathbf{d}(k) \end{bmatrix} \in \mathbb{R}^{n_f + n_p}. \tag{65}$$

The resulting augmented discrete-time system model employed by the MPC is given by

$$\begin{aligned} \mathbf{x}_{f_A}(k+1) &= \underbrace{\begin{bmatrix} \mathbf{A}_{f_d} & \mathbf{E}_{f_d}\mathbf{C}_\xi \\ \mathbf{0} & \mathbf{\Gamma}_\xi \end{bmatrix}}_{\mathbf{A}_{f_A}} \mathbf{x}_{f_A}(k) + \underbrace{\begin{bmatrix} \mathbf{B}_{f_d} \\ \mathbf{0} \end{bmatrix}}_{\mathbf{B}_{f_A}} u(k), \\ y_f(k) &= \underbrace{\begin{bmatrix} \mathbf{C}_{f_d} & \mathbf{0} \end{bmatrix}}_{\mathbf{C}_{f_A}} \mathbf{x}_{f_A}(k), \end{aligned} \tag{66}$$

where $\mathbf{C}_\xi \in \mathbb{R}^{1 \times n_p}$ extracts the generalized disturbance from $\mathbf{d}(k)$:

$$\xi(k) = \mathbf{C}_\xi \mathbf{d}(k) \tag{67}$$

with $\mathbf{C}_\xi \in \mathbb{R}^{1 \times n_p}$ defined as

$$\mathbf{C}_\xi = \begin{bmatrix} 1 & 0 & \cdots & 0 \end{bmatrix}, \tag{68}$$

with $n_p = p + 1$.

This augmented model serves as the prediction model within the MPC optimization problem, allowing the controller to anticipate and compensate the future effect of time-varying load torque disturbances through the embedded polynomial dynamics.

4.4.3. Disturbance Estimation via Kalman Filter Design

To enable online disturbance estimation within the MPC framework, the augmented flat-state vector $\mathbf{x}_{f_A}(k)$ is estimated from the measured output $y_f(k)$ using a discrete-time Kalman filter [41,42], with the following stochastic estimation model:

$$\begin{aligned} \mathbf{x}_{f_A}(k+1) &= \mathbf{A}_{f_A}\mathbf{x}_{f_A}(k) + \mathbf{B}_{f_A}u(k) + \mathbf{w}(k), \\ y_f(k) &= \mathbf{C}_{f_A}\mathbf{x}_{f_A}(k) + v(k), \end{aligned} \tag{69}$$

where $\mathbf{w}(k)$ and $v(k)$ are zero-mean, mutually uncorrelated process and measurement noise sequences with covariance matrices $\mathbf{Q}_w \succeq \mathbf{0}$ and $R_v \succ 0$, respectively. The matrices $\mathbf{A}_{f_A}$, $\mathbf{B}_{f_A}$ and $\mathbf{C}_{f_A}$ follow from (66).

Given the estimate $\hat{\mathbf{x}}_{f_A}(k|k)$ and its error covariance $\mathbf{P}(k|k)$, the Kalman filter recursion is computed as follows, with the prediction defined as

$$\begin{aligned} \hat{\mathbf{x}}_{f_A}(k+1|k) &= \mathbf{A}_{f_A}\hat{\mathbf{x}}_{f_A}(k|k) + \mathbf{B}_{f_A}u(k), \\ \mathbf{P}(k+1|k) &= \mathbf{A}_{f_A}\mathbf{P}(k|k)\mathbf{A}_{f_A}^{\top} + \mathbf{Q}_w, \end{aligned} \tag{70}$$

and the correction step is obtained from the innovation covariance and Kalman gain

$$\begin{aligned} \mathbf{S}(k+1) &= \mathbf{C}_{f_A}\mathbf{P}(k+1|k)\mathbf{C}_{f_A}^{\top} + R_v, \\ \mathbf{K}(k+1) &= \mathbf{P}(k+1|k)\mathbf{C}_{f_A}^{\top}\mathbf{S}(k+1)^{-1}, \end{aligned} \tag{71}$$

leading to the updated estimate

$$\begin{aligned} \hat{\mathbf{x}}_{f_A}(k+1|k+1) &= \hat{\mathbf{x}}_{f_A}(k+1|k) + \mathbf{K}(k+1)\Big[y_f(k+1) - \mathbf{C}_{f_A}\hat{\mathbf{x}}_{f_A}(k+1|k)\Big], \\ \mathbf{P}(k+1|k+1) &= \Big(\mathbf{I} - \mathbf{K}(k+1)\mathbf{C}_{f_A}\Big)\mathbf{P}(k+1|k). \end{aligned} \tag{72}$$

The estimated disturbance is reconstructed from the estimated polynomial disturbance state as

$$\hat{\xi}(k) = \mathbf{C}_{\xi}\,\hat{\mathbf{d}}(k|k), \tag{73}$$

where $\hat{\mathbf{d}}(k|k)$ denotes the disturbance subvector of $\hat{\mathbf{x}}_{f_A}(k|k)$. The estimated augmented state $\hat{\mathbf{x}}_{f_A}(k|k)$ is supplied to the MPC as the initial condition of the prediction horizon.

The augmented formulation allows the MPC to incorporate the estimated disturbance state $\hat{\xi}$ directly into its prediction model as portrayed by the scheme in Figure 2. As a result, load torques are effectively compensated, ensuring offset-free tracking without requiring explicit differentiation of the load torque or detailed modelling of the disturbance.

The estimator converges to the applied torque disturbance, providing the controller with the necessary information to preserve tracking performance. By explicitly embedding the estimated disturbance dynamics into the predictive model, the MPC anticipates the future impact of dynamic load torques and compensates their effects through the optimized control action. As a result, offset-free tracking performance is preserved while robustness against considerably fast varying and oscillatory disturbances is significantly enhanced.

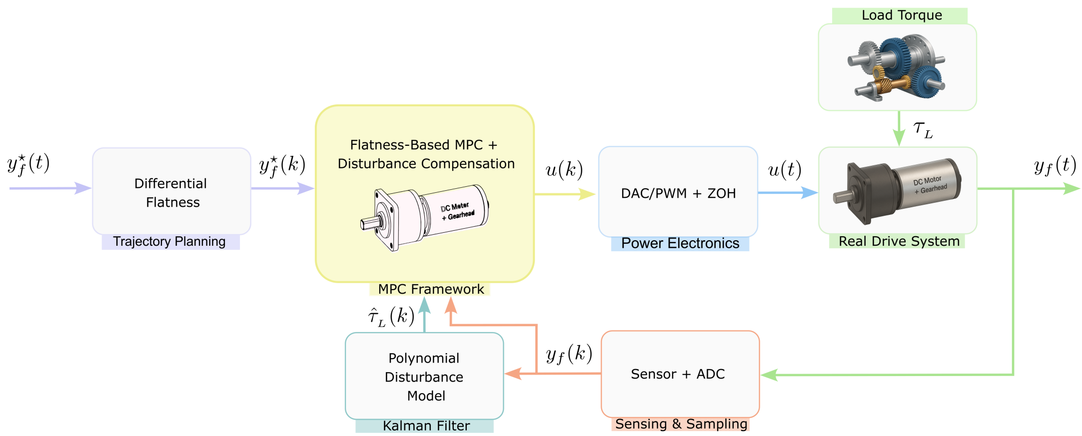

Figure 2. Main block diagram of the proposed flatness-based MPC framework with polynomial load torque disturbance estimation.

4.5. Controller Tuning and Implementation Parameters

To provide a clear description of the proposed control framework, this subsection presents the tuning parameters employed for both the MPC and the Kalman filter-based disturbance estimator including the weighting matrices, prediction horizon, as well as the covariance matrices and initialization conditions of the Kalman filter.

It is worth mentioning that parameter selection was carried out based on the trade-off between tracking performance, control effort, and estimation accuracy, and was kept consistent across all evaluated scenarios. The tuning parameters were selected heuristically through iterative numerical experimentation to achieve a suitable balance between tracking performance, control effort, and estimation accuracy.

The MPC weighting matrices were selected to prioritize accurate tracking performance while maintaining a moderate control effort. After several numerical experiments, the prediction horizon was set to $N = 100$, providing sufficient anticipation of the system dynamics and disturbance effects without significantly increasing computational complexity.

On the other hand, a relatively large value was assigned to $\mathbf{Q}_y = \mathrm{diag}(1 \times 10^5)$ to prioritize output tracking accuracy, while a smaller value was used in $\mathbf{Q}_u = \mathrm{diag}(1)$ to avoid excessive penalization of the control action. The augmented model used for control design consists of $n_x = 3$ states, with a single control input $n_u = 1$ and a single measured output $n_r = 1$. Accordingly, the input weighting matrix $\mathbf{Q}_u \in \mathbb{R}^{n_u \times n_u}$ reduces to a scalar-valued diagonal matrix.

Regarding the state estimation, the Kalman filter covariance matrices were tuned according to the relative importance of the system states and the disturbance dynamics. During the design stage, larger values were assigned to the disturbance-related components in $\mathbf{Q}_w$ and $\mathbf{P}(0)$ to enhance the estimator adaptability to time-varying load torque conditions.

In contrast, smaller values were used for the physical states to reflect higher confidence in the system model, as shown in (74) and (75), which correspond to the process noise covariance and the initial estimation covariance, respectively. In addition, the measurement noise covariance was set as $R_v = \sigma_y^2 = (0.015)^2 = 2.25 \times 10^{-4}$, where σ_y is the standard deviation of the injected measurement noise.

$$\mathbf{Q}_w = \mathrm{diag}\left(10^{-8}, 10^{-8}, 10^{8}, 10^{6}, 10^{4}, 10^{2}, 10^{0}\right), \tag{74}$$

$$\mathbf{P}(0) = \mathrm{diag}\left(10^{-4}, 10^{-4}, 10^{10}, 10^{8}, 10^{6}, 10^{4}, 10^{2}\right). \tag{75}$$

The augmented state vector, including the disturbance-related states, is initialized to zero, i.e., $\hat{\mathbf{x}}_{f_A}(0) = \mathbf{0}$, while the large covariance values in $\mathbf{P}(0)$ allow the Kalman filter to rapidly adapt the disturbance estimates.

From an implementation perspective, the resulting MPC problem is formulated as a quadratic program with a standard structure, which can be efficiently solved using available numerical routines. The relatively low dimension of the augmented model, together with the use of a single-input configuration, leads to a compact optimization problem.

Furthermore, due to the differential flatness-based parametrization, the control scheme relies only on the velocity measurement, avoiding the need for additional state measurements nor observers. These characteristics support the suitability of the proposed approach for real-time implementation.

4.6. Sensitivity Analysis of the Polynomial Disturbance Order

The polynomial disturbance model order was selected as $p = 4$ based on a trade-off between representation capability and computational complexity and formalized by developing a sensitivity analysis. The reference was kept constant and the same load torque profile and measurement noise sequence were applied for all polynomial orders.

The analysis was performed by varying the polynomial disturbance order p and evaluating its effect on the disturbance reconstruction performance as portrayed in Figure 3 and summarized in Algorithm 1, where some quantitative metrics were adopted: the root mean square error to provide a global measure of estimation accuracy with higher sensitivity to large deviations,

$$\mathrm{RMSE}_\tau = \sqrt{\frac{1}{N}\sum_{k=1}^{N} e_\tau^2(k)}.$$

Algorithm 1 Sensitivity analysis of the polynomial disturbance order.

1: Generate base signals using a fixed disturbance profile and noise realization.
2: **for** $p = 0$ to $p_{\max}$ **do**
3: Initialize Kalman filter with polynomial order p.
4: **for** $k = 1$ to N **do**
5: Update Kalman filter using $u(k)$ and $y_f(k)$.
6: Estimate disturbance $\hat{\tau}_L(k)$.
7: **end for**
8: Compute performance metrics: RMSE, MAE, $e_{\max}$ and STD.
9: **end for**
10: Compare results across different values of p.

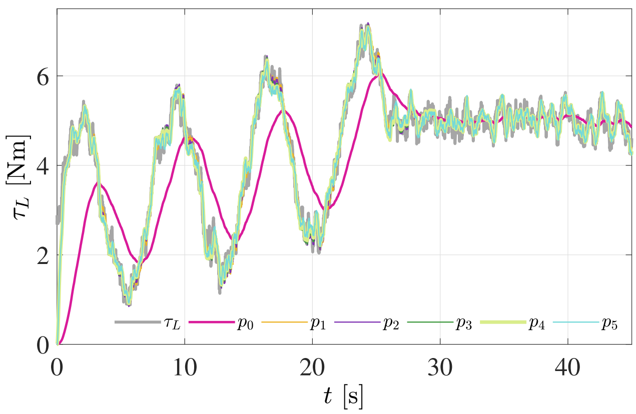

Figure 3. Polynomial-order sensitivity in disturbance estimation.

Meanwhile, the mean absolute error reflects the average magnitude of the error of estimation:

$$\mathrm{MAE}_\tau = \frac{1}{N}\sum_{k=1}^{N} |e_\tau(k)|,$$

the maximum error $e_{\max}$ captures the worst-case deviation during transient behaviour,

$$e_{\max,\tau} = \max_k |e_\tau(k)|,$$

and the standard deviation

$$\mathrm{STD}_\tau = \mathrm{std}(e_\tau(k)),$$

evaluates the variability of the estimation error, indicating the level of oscillations or noise amplification. Note the subscript τ indicates that all performance metrics are computed based on the load torque estimation error defined as

$$e_\tau(k) = \tau_L(k) - \hat{\tau}_L(k).$$

As shown in Table 1 and Figure 3, all metrics exhibit a significant improvement when increasing the polynomial order from $p = 0$ to $p = 1$. However, for $p \geq 2$, the variations in all metrics become marginal, indicating that the disturbance reconstruction performance reaches a saturation point.

In this case, this quantitative evidence supports the selection of $p = 4$ as a suitable compromise between reconstruction accuracy and estimator complexity. It is worth mentioning the disturbance covariance matrix was scaled accordingly to p, assigning progressively smaller process noise to higher-order components while maintaining a consistent tuning strategy.

Table 1. Sensitivity analysis of the polynomial disturbance order based on estimation performance.

p_i	RMSE_τ	MAE_τ	$e_{\max,\tau}$	STD_τ
0	1.0748	0.7593	3.9094	1.0523
1	0.2675	0.1816	2.8850	0.2672
2	0.2640	0.1780	2.8850	0.2636
3	0.2630	0.1770	2.8850	0.2626
4	**0.2626**	**0.1766**	**2.8850**	**0.2622**
5	0.2626	0.1764	2.8850	0.2621

5. Numerical Results and Comparative Analysis

In this section, numerical experiments are carried out using the electromechanical system composed by the Maxon® DC 218009 motor with nominal speed 4920 rpm (515.2211 rad/s), coupled with a Planetary Gearhead GP 52 Ceramic from Maxon® with a reduction ratio of 81:1; then, the nominal output speed of the system is 6.36 rad/s.

Henceforth, the effectiveness of the proposed MPC framework against the PID, LQI and off-set free MPC control architectures is validated in the presence of disturbances and noisy measurements. The parameters of the system are listed in Table 2.

Table 2. System parameters.

Parameter	Symbol	Value	Units
Back electromotive force constant	k_e	82.321	mV/rad/s
Motor torque constant	k_m	82.2	mN·m/A
Resistance	R	0.651	Ω
Inductance	L	0.612	mH
System equivalent inertia moment	J_e	2.4	kg·m^2
System equivalent viscous damping	b_e	6.562	N·m·s/rad
Gear reduction ratio	η	81	–

The controllers are implemented, validated, and compared using the following three realistic scenarios:

1. System subjected to constant load torque disturbance.
2. System subjected to time-varying disturbing load torque with stochastic components.
3. System performance under different sampling times for the second case.

Polynomial Bézier interpolations described by the expressions (76) and (77) are implemented for the smooth transient responses between initial and desire speed values of the DC motor-gearhead drive system

$$y_f^\star(t) = \begin{cases} \Omega_i, & 0 \le t < T_i, \\ \Omega_i + \left(\Omega_f - \Omega_i\right)\mathcal{B}_z(t, T_i, T_f), & T_i \le t \le T_f, \\ \Omega_f, & t > T_f, \end{cases} \tag{76}$$

where Ω_i and Ω_f stand for the initial and final speed reference values, whilst T_i and T_f are the times when the transition begins and ends, respectively. In this regard,

$$\mathcal{B}_z(t, T_i, T_f) = \sum_{j=1}^{6} \mu_j \left(\frac{t - T_i}{T_f - T_i}\right)^j, \tag{77}$$

with $\mu_1 = 252$, $\mu_2 = 1050$, $\mu_3 = 1800$, $\mu_4 = 1575$, $\mu_5 = 700$, and $\mu_6 = 126$.

In addition to the fact that the control design and control actions are computed in discrete time and applied to the plant through a zero-order hold, the system response is shown in continuous time for clarity. Moreover, dashed lines in the figures denote reference trajectories planned for system operation whereas the solid lines are used for system variables.

Additionally, to properly evaluate the system response by implementing the previously introduced control schemes in the three-case study, diverse performance metric indexes are computed based on the tracking error $e(k)$ and the control input $u(k)$ at the discrete-time instant k.

The implemented metric criteria are widely implemented in the control systems literature [6,36,43–46] and highlight different aspects of the closed-loop performance in terms of tracking accuracy and control effort.

The normalized root mean square error evaluates the average magnitude of the tracking error over the time horizon and normalized with respect to the reference signal representing a measure of overall tracking accuracy and which is computed as follows:

$$\text{NRMSE} = \frac{\sqrt{\phi}}{y^\star_{\max} - y^\star_{\min}}, \tag{78}$$

where $y^\star_{\max}$ and $y^\star_{\min}$ represent the maximum and minimum values of the reference signal over the evaluation horizon, e denotes the difference between the desired and real output and

$$\phi = \frac{1}{N}\sum_{k=0}^{N} e(k)^2. \tag{79}$$

The cumulative tracking error is evaluated through the integral of absolute error as follows:

$$\text{IAE} = \sum_{k=0}^{N} |e(k)|\, T_s, \tag{80}$$

and the steady-state and transient tracking errors are penalized using the integral of time-weighted absolute error,

$$\text{ITAE} = \sum_{k=0}^{N} kT_s\, |e(k)|\, T_s, \tag{81}$$

both of which are classical performance criteria in control system analysis. Finally, for complementing the performance evaluation, control effort and smoothness are assessed using discrete-time metrics computed directly from the applied control signal and based on $\mathcal{L}_2$ norm.

The discrete version of the $\mathcal{L}_2$ norm of the control input signal provides a compact measure of the overall control effort applied to the system,

$$\|u\|_2 = \left[\sum_{k=0}^{N} u(k)^2\right]^{\frac{1}{2}}, \tag{82}$$

while the time-normalized $\mathcal{L}_2$ rate of control increments quantifies control smoothness by penalizing rapid variations in the control signal.

$$\|\Delta u\|_2 = \left[\frac{1}{T}\sum_{k=1}^{N} \left[u(k) - u(k-1)\right]^2\right]^{\frac{1}{2}}, \tag{83}$$

where T denotes the total evaluation time.

5.1. Case I: Output System Response Subjected Constant Load Torque

To highlight the system response by using the proposed MPC framework, the system response is evaluated numerically when subjected to a constant disturbing load torque.

Figures 4 and 5 show that, although all controllers achieve proper output tracking, the proposed MPC framework with polynomial disturbance estimation further reduces both accumulated and long-term tracking errors, as evidenced by lower IAE and ITAE values, without increasing control effort or input variations. Note from Figure 5, under not extreme operational conditions such as a constant load torque and noise-free measurements, the LQI controller achieves acceptable disturbance compensation and offset-free tracking. Moreover, despite the fact that an adequate performance of the system is exhibited when adopting the feed-forward PID-like controller or the offset-free MPC, the proposed MPC framework provides improved transient behaviour when a load torque of magnitude 3.5 [Nm] is abruptly applied eight seconds after start the motion.

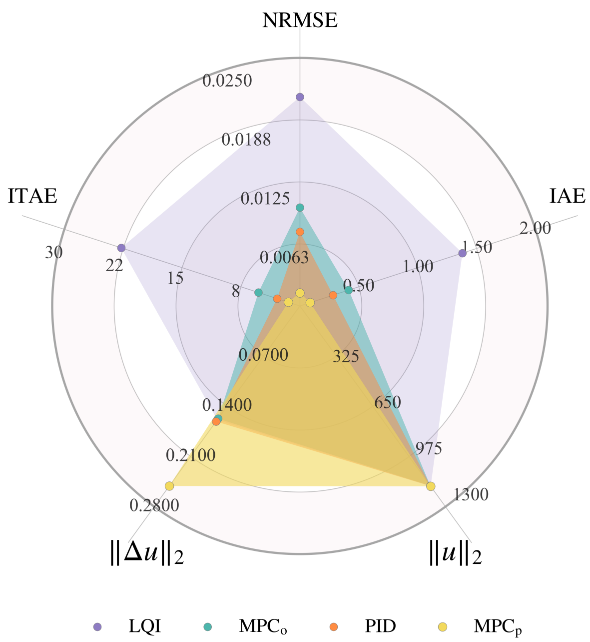

Figure 4. Radar plot for quantitative comparison of tracking performance and control effort in Case I.

In the radar plots, the nominal offset-free MPC response is represented by MPC_o, whereas the MPC enhanced with polynomial disturbance estimation is represented by MPC_p.

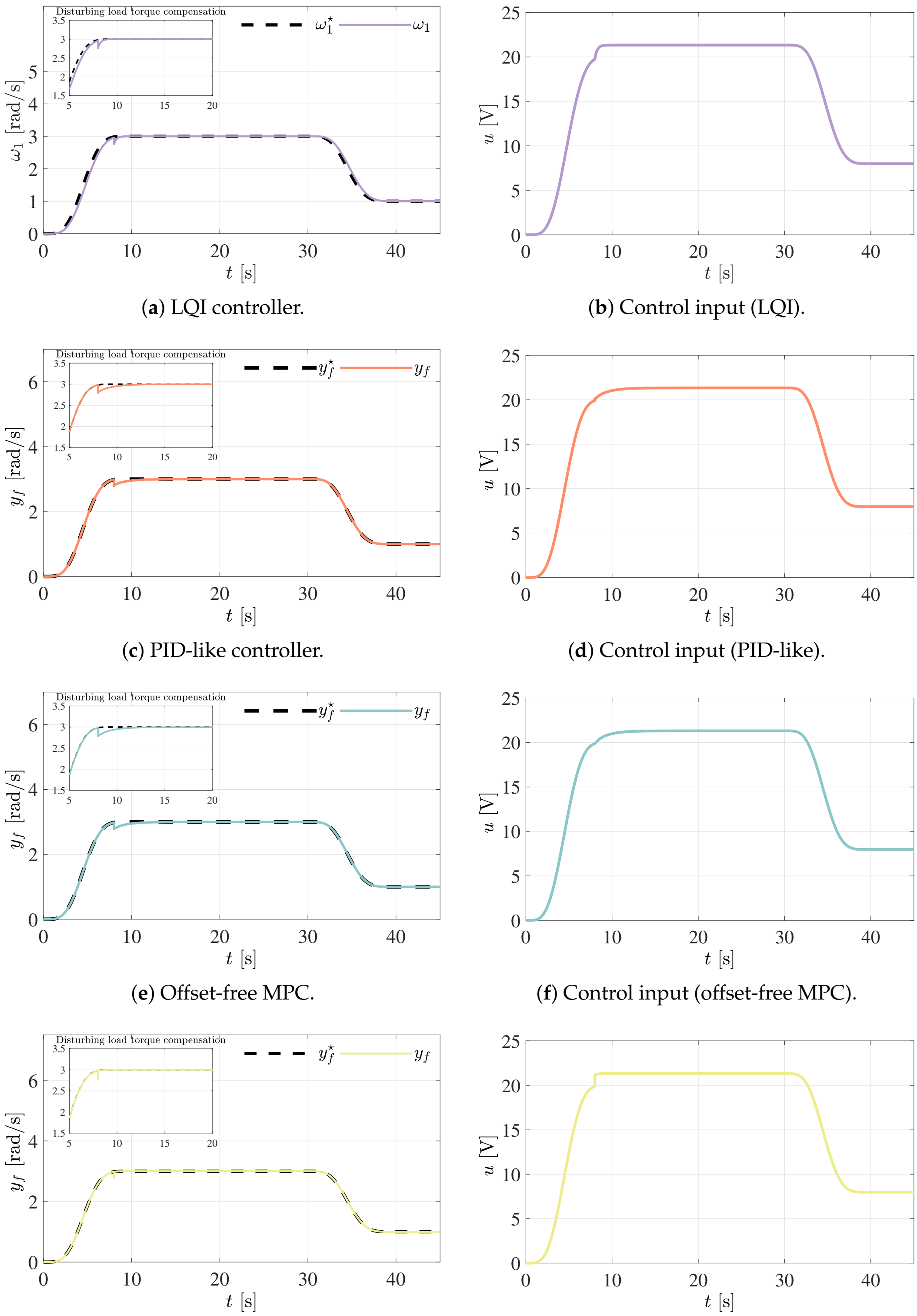

(**a**) LQI controller. (**b**) Control input (LQI).

(**c**) PID-like controller. (**d**) Control input (PID-like).

(**e**) Offset-free MPC. (**f**) Control input (offset-free MPC).

(**g**) Proposed MPC framework. (**h**) Control input (proposed MPC).

Figure 5. Closed-loop responses under a constant load torque disturbance (Case I). The left column shows output tracking performance, while the right column presents the corresponding control inputs. Insets highlight the transient behaviour.

As shown in the zoomed-in views provided by the insets, the system recovers faster from the perturbation with the proposed MPC framework and without inducing control input saturation. Figure 6 presents the disturbance torque estimation by the MPC-based approaches. Although the offset-free MPC is able to accurately estimate the constant but completely unknown load torque, the proposed MPC with polynomial disturbance estimation achieves superior performance, which is consistently reflected in the quantitative plot portrayed in Figure 4.

Table 3 presents the quantitative performance metrics obtained in Case I, providing a detailed comparison of tracking accuracy and control effort among the evaluated control strategies. While the LQI controller achieves acceptable tracking performance, it requires a significantly higher control effort, as indicated by the largest values of $\|u\|_2$ and ITAE. The PID-like controller reduces the control effort but exhibits inferior tracking robustness while the offset-free MPC provides a better balance between tracking accuracy and control effort. However, the proposed MPC framework consistently outperforms the remaining controllers by achieving the lowest tracking error evidenced by the related indices, a trend that is clearly confirmed by the normalized bar plot in Figure 7.

Table 3. Quantitative performance metrics for Case I.

Controller	NRMSE	IAE	$\|u\|_2$	$\|\Delta u\|_2$	ITAE
LQI	0.021	1.380	1167.550	0.159	22.745
PID	0.008	0.282	1165.490	0.161	2.894
MPC_o	0.010	0.415	1164.150	0.157	5.279
MPC_p	0.001	0.087	1168.010	0.251	1.470

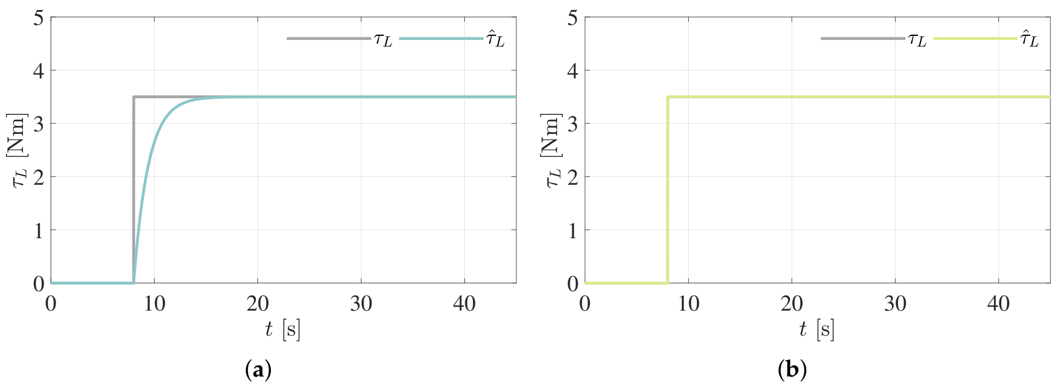

Figure 6. Load torque disturbance estimation in Case I. The true disturbance τ_L and its estimate $\hat{\tau}_L$ are shown for (**a**) offset-free MPC and (**b**) the proposed MPC framework.

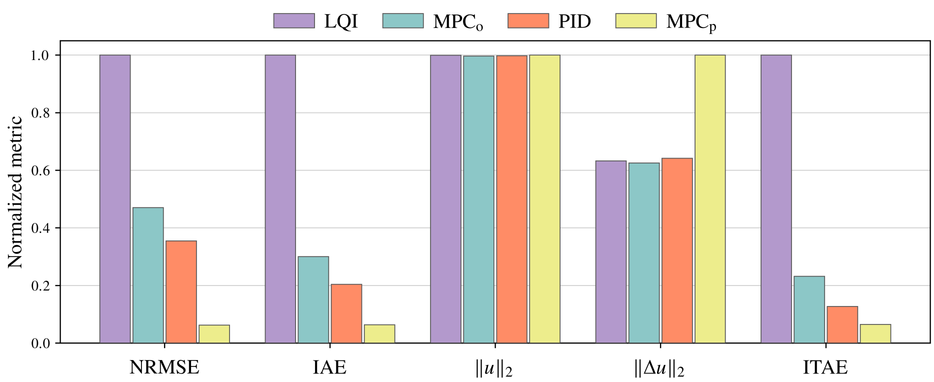

Figure 7. Normalized performance comparison in Case I.

The normalized values are computed for each performance metric m_j ($j = 1, \ldots, 5$) and controller i as follows:

$$\bar{m}_{i,j} = \frac{m_{i,j}}{\max\limits_{k \in \mathcal{C}} m_{k,j}}, \tag{84}$$

where $\mathcal{C} = \{\text{LQI}, \text{PID}, \text{MPC}_\text{o}, \text{MPC}_\text{p}\}$ denotes the set of evaluated controllers. This normalization preserves the *lower-is-better* interpretation of all metrics on a unified scale, enabling a direct and clear visual comparison of the relative performance across controllers in the bar charts. It is worth mentioning that the same sampling time and input saturation limits are adopted for the assessment of the four control approaches.

In the next section, noisy measurements of the controlled output are included to assess the capability of each strategy to cope with measurement disturbances. In addition, to emphasize the intrinsic sensitivity of classical optimal controllers to discretization effects, the weighting matrices are kept unchanged when varying T_s, while the MPC-based formulations naturally adapt through their prediction model and horizon definition.

5.2. Case II: Output System Response Subjected Time-Varying Load Torque with $T_s = 10$ *ms*

To assess the system response under dynamic load torque disturbances and measurement noise using the proposed MPC framework, the numerical experiments in Case II and Case III considers the following disturbance profile

$$\tau_\text{b}(t) = \tau_0 + \alpha_1 t + \alpha_2 t^2 + A_\tau \sin(\omega t) + c_\tau, \tag{85}$$

where the constant offset, ramp, quadratic, and oscillatory components are specified as $\tau_0 = 2.0$ Nm, $\alpha_1 = 0.05$ N m/s, $\alpha_2 = 0.001$ N m/s^2, $A_\tau = 2.0$ Nm, and $\omega = 0.85$ rad/s. The constant term c_τ is selected such that $\tau_\text{b} \approx \tau_\text{c}$ at the switching instant t_sw, thus avoiding discontinuities in the applied disturbance torque. Thus, the overall torque acting on the system is then defined as

$$\tau(t) = \begin{cases} \tau_\text{b}(t), & t < t_\text{sw}, \\ \tau_\text{c}, & t \geq t_\text{sw}, \end{cases} \tag{86}$$

with switching time $t_\text{sw} = 25.75$ s and constant torque level $\tau_\text{c} = 5$ Nm. The continuous-time load torque profile $\tau(t)$ is discretized by uniform sampling with period T_s, yielding the discrete-time sequence $\tau(k) = \tau(kT_s)$, which is used for numeric experiments.

In addition, an unmodelled stochastic mechanical disturbance term is incorporated into the nominal torque through an autoregressive process model [47] of order one,

$$\tau_\text{n}(k) = \alpha_\tau \tau_\text{n}(k-1) + \beta_\tau w(k), \qquad w(k) \sim \mathcal{N}(0, 1), \tag{87}$$

where $\alpha_\tau = 0.94$ and $\beta_\tau = \sigma_\tau \sqrt{1 - \alpha_\tau^2}$, with $\sigma_\tau = 0.25$ Nm. The resulting applied load torque is then given by

$$\tau_L(k) = \tau(k) + \tau_\text{n}(k). \tag{88}$$

Finally, zero-mean Gaussian noise is added to corrupt the velocity output signal measurement with standard deviation $\sigma_y = 0.015$ rad/s,

$$y_\text{m}(k) = y(k) + n_y(k), \qquad n_y(k) \sim \mathcal{N}(0, \sigma_y^2). \tag{89}$$

In Figures 8 and 9 it is portrayed the results in Case II. The plots evidence a better tracking of the speed reference trajectory by means of the proposed MPC framework even in the presence of oscillatory terms in the time-varying load torque.

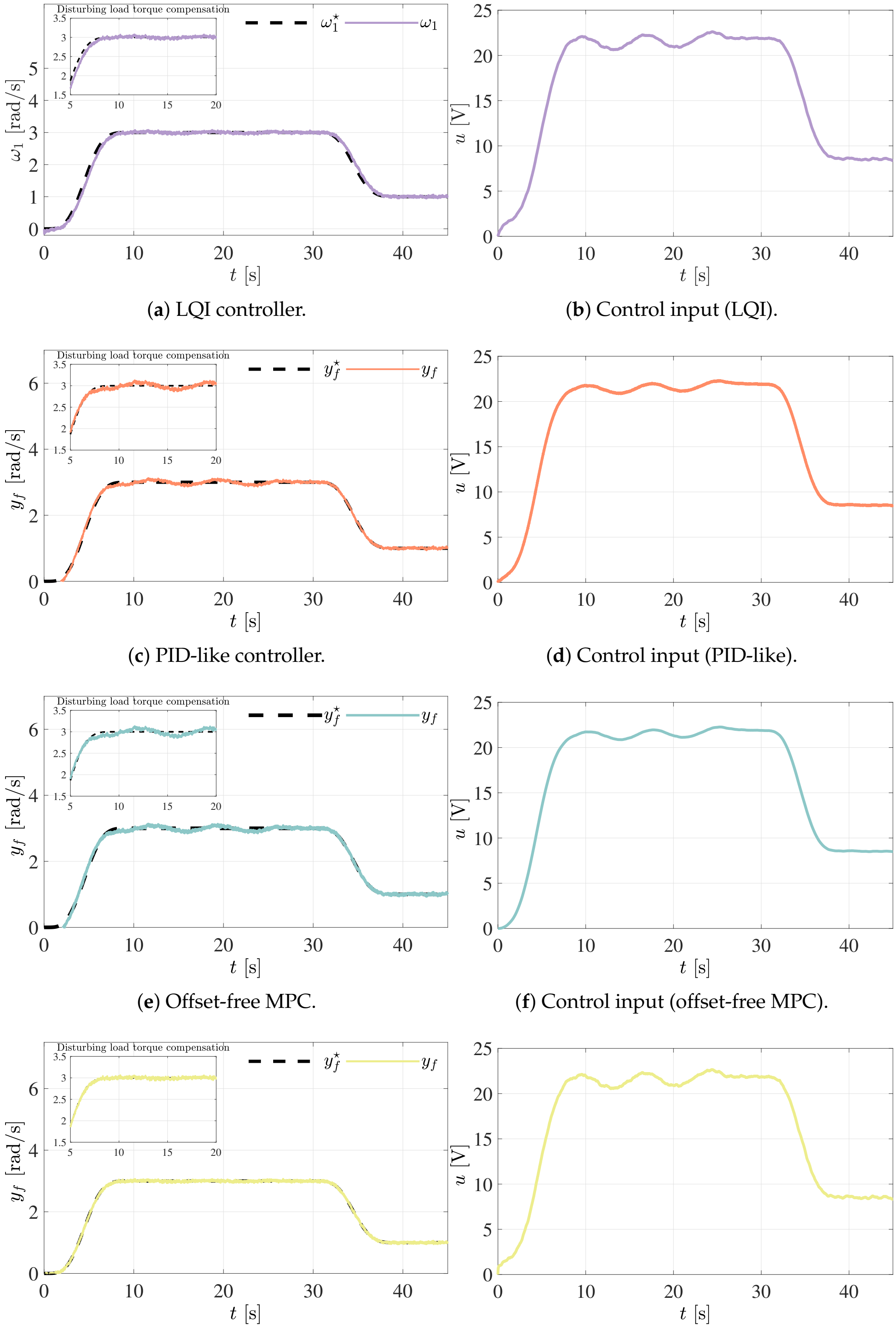

(**a**) LQI controller. (**b**) Control input (LQI).

(**c**) PID-like controller. (**d**) Control input (PID-like).

(**e**) Offset-free MPC. (**f**) Control input (offset-free MPC).

(**g**) Proposed MPC framework. (**h**) Control input (proposed MPC).

Figure 8. Closed-loop responses under a load torque disturbance with a sampling time of 10 ms. The left column shows output tracking performance, while the right column presents the corresponding control inputs. Insets highlight the transient behaviour.

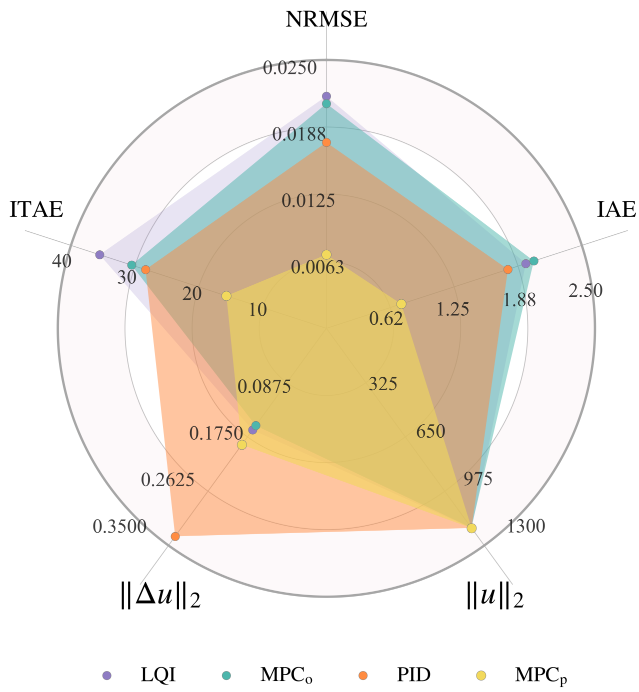

Figure 9. Radar plot for quantitative comparison of tracking and control effort in Case II.

Moreover, the output measurements, corrupted by stochastic and sensor noise, are effectively processed by the Kalman filter, enabling accurate state estimation without inducing excessive control activity, as shown in Figures 10 and 11. As a result, the proposed framework maintains a favourable balance between tracking accuracy and control smoothness under noisy and uncertain scenarios.

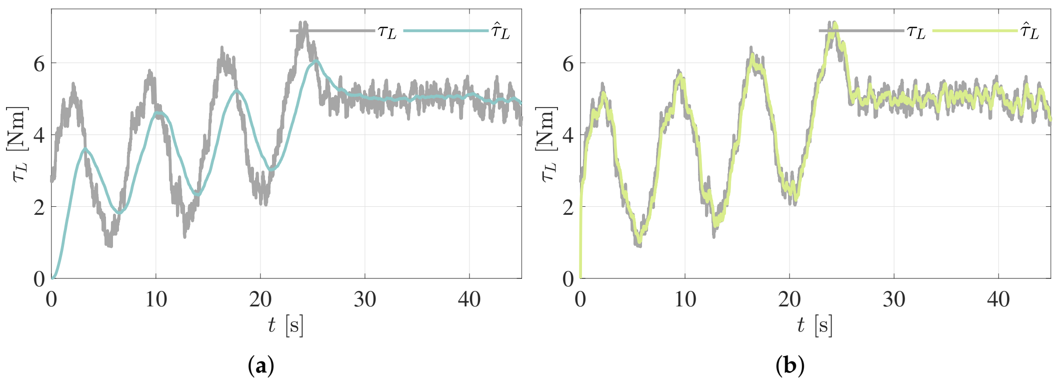

Figure 10. Load torque disturbance estimation in Case II. The true disturbance τ_L and its estimate $\hat{\tau}_L$ are shown for (**a**) offset-free MPC and (**b**) the proposed MPC framework.

Table 4 and Figure 11 indicate that the LQI and PID controllers exhibit larger tracking errors and higher ITAE values under oscillatory load torque conditions, reflecting a reduced disturbance rejection capability. The offset-free MPC improves tracking accuracy but at the expense of increased cumulative error. In contrast, the proposed MPC framework attains the lowest tracking-related metrics while preserving a comparable control effort, evidencing a better trade-off between performance and smoothness.

Table 4. Quantitative performance metrics for Case II.

Controller	NRMSE	IAE	$\|\|u\|\|_2$	$\|\|\Delta u\|\|_2$	ITAE
LQI	0.022	1.952	1196.132	0.164	35.507
PID	0.017	1.777	1195.189	0.335	28.322
MPC_o	0.021	2.030	1193.609	0.157	30.501
MPC_p	0.007	0.733	1196.051	0.188	15.663

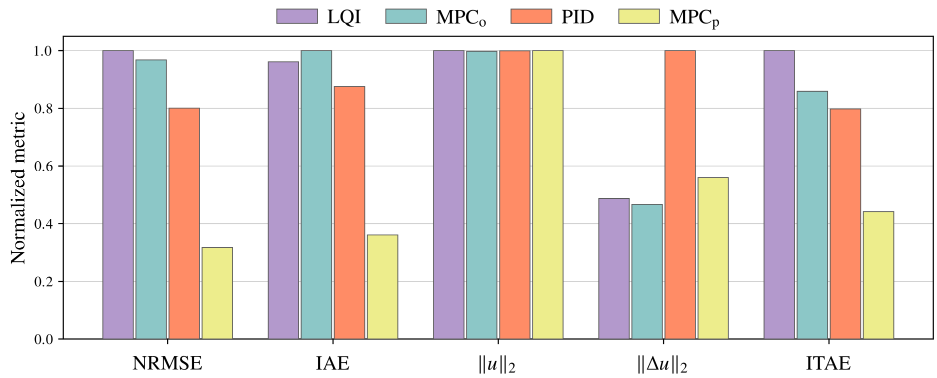

Figure 11. Normalized performance comparison in Case II.

5.3. Case III: Output System Response Subjected Time-Varying Load Torque with $T_s = 1$ ms

Finally, the system response is evaluated considering a sampling time of $T_s = 1$ ms and subjected to the load torque defined in (88). It is worth noting that the sampling period T_s directly impacts the closed-loop performance, particularly under fast-varying disturbances.

As illustrated in Figures 12 and 13, a reduction in T_s increases the sensitivity of classical controllers to measurement noise and oscillatory disturbance components. In this scenario, the proposed MPC framework consistently achieves the lowest tracking error indices among all controllers, even under fast sampling and time-varying disturbances. While the LQI and PID controllers exhibit comparable control energy levels, their performance deteriorates in terms of tracking accuracy and robustness, which is reflected in higher ITAE values.

The quantitative results reported in Table 5 and summarized by the normalized bar chart in Figure 14 further support the previous observations. Simultaneously, the offset-free MPC improves disturbance rejection compared to classical controllers, but remains less effective than the proposed MPC framework when dealing with significantly fast-varying disturbances, as evidenced in Figure 15, and by the higher error-related metrics and smoother but less accurate response.

An important advantage of the proposed approach is that no re-tuning is required when transitioning between the considered operating scenarios. The same MPC weights and constraints are retained across all cases while a good performance is preserved by explicitly incorporating the estimated disturbance into the MPC prediction model. As a result, the proposed framework provides improved speed tracking, effective disturbance rejection, and smoother control action for DC motor–gearhead drive systems operating under uncertain, time-varying loads and noisy measurements.

Case III highlights the core contribution of this work. Under a fast sampling regime and in the presence of dynamic and stochastic load torque disturbances, the proposed framework fully exploits the flat system representation together with the polynomial filter to preserve prediction accuracy.

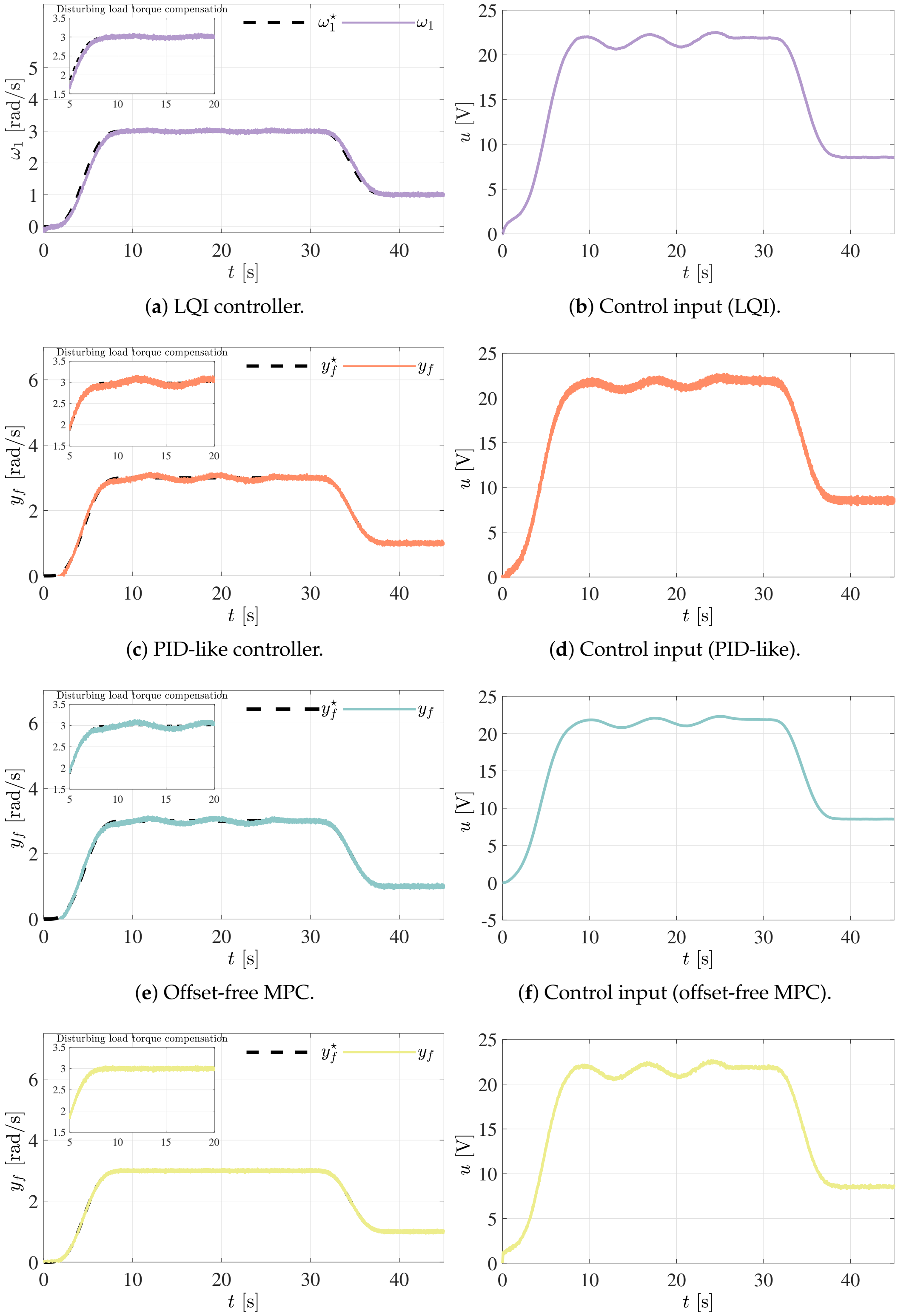

(**a**) LQI controller.

(**b**) Control input (LQI).

(**c**) PID-like controller.

(**d**) Control input (PID-like).

(**e**) Offset-free MPC.

(**f**) Control input (offset-free MPC).

(**g**) Proposed MPC framework.

(**h**) Control input (proposed MPC).

Figure 12. Closed-loop responses under a load torque disturbance with a sampling time of 1 ms. The left column shows output tracking performance, while the right column presents the corresponding control inputs. Insets highlight the transient behaviour.

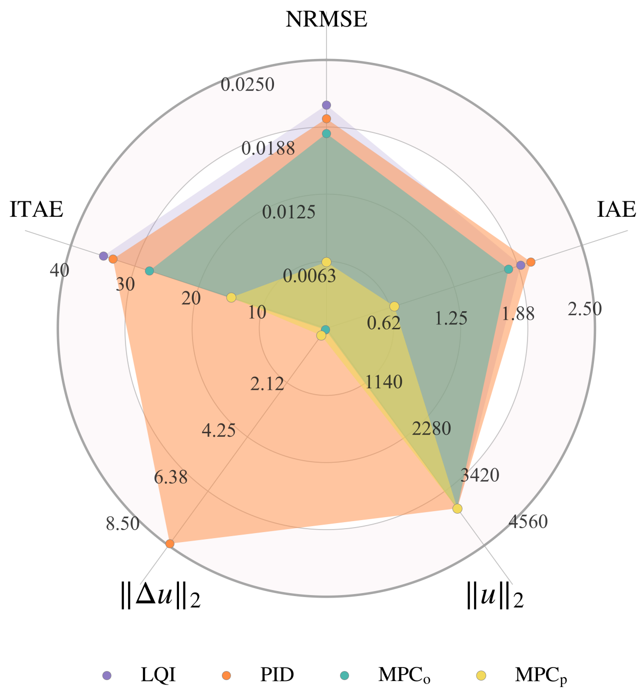

Figure 13. Radar plot for quantitative comparison of tracking and control effort in Case III.

Unlike conventional controllers, where disturbance effects are treated as external or lumped uncertainties, the proposed approach explicitly incorporates the estimated disturbance dynamics into the MPC prediction model. This results in improved tracking accuracy, reduced performance degradation, and an acceptable trade-off between control effort and smoothness, as reflected by the quantitative metrics.

Table 5. Quantitative performance metrics for Case III.

Controller	NRMSE	IAE	$\|u\|_2$	$\|\Delta u\|_2$	ITAE
LQI	0.021	1.902	3783.428	0.059	34.919
PID	0.020	2.001	3779.995	8.429	33.428
MPC$_o$	0.018	1.783	3778.084	0.049	27.711
MPC$_p$	0.006	0.664	3783.393	0.276	14.911

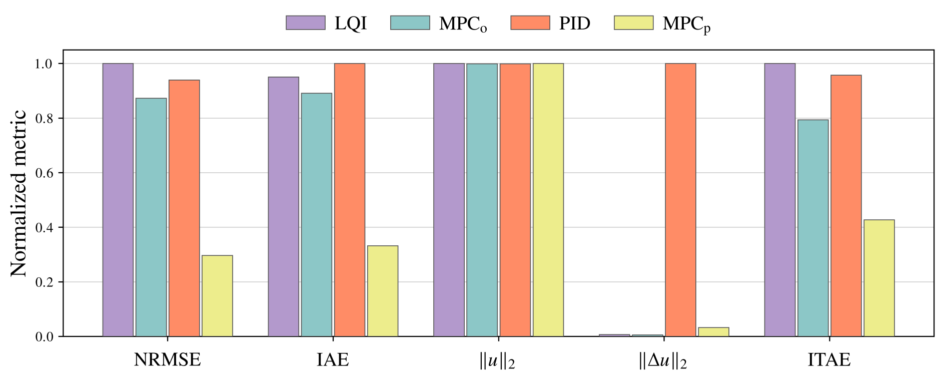

Figure 14. Normalized performance comparison in Case III.

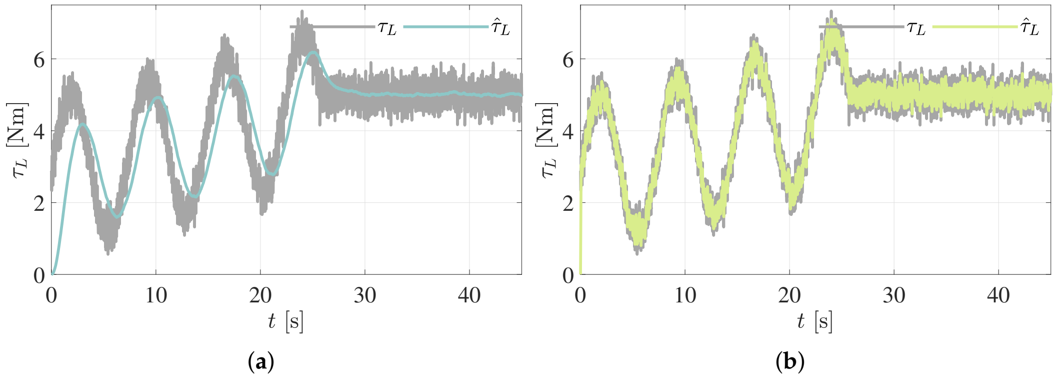

Figure 15. Load torque disturbance estimation in Case III. The true disturbance τ_L and its estimate $\hat{\tau}_L$ are shown for (**a**) offset-free MPC and (**b**) the proposed MPC framework.

In Case III, the proposed MPC framework confirms improved tracking performance, as indicated by lower NRMSE and IAE values compared to the other controllers. The reduction in ITAE evidence a faster and effective transient response under time-varying disturbances. While the control effort remains comparable, a higher variation in the control input (Δu) is observed, reflecting the controller's increased responsiveness to disturbance effects. Note that despite the reactive response, the control action remains bound by design due to the constraints explicitly enforced within the MPC formulation.

5.4. Discussion and Limitations

The quantitative results reported in Tables 3–5 and the normalized comparisons in Figures 7, 11 and 14 complement the visual analysis of the closed-loop responses. In all evaluated scenarios, the proposed MPC framework achieves the lowest tracking-related indices, particularly NRMSE, IAE, and ITAE, which confirms an improvement in tracking accuracy and a faster recovery under disturbance effects. In Case I, the proposed controller provides a better compensation of the constant load torque disturbance. In Cases II and III, where time-varying load torques, stochastic components, and measurement noise are considered, the reduction in these metrics becomes more evident, showing the advantage of embedding the polynomial disturbance estimate into the MPC prediction model.

Although the proposed framework may produce a larger control input variation in some scenarios, the overall control effort remains comparable to the other evaluated controllers. This behaviour reflects the increased responsiveness of the controller to dynamic disturbance changes, while the control signal remains bounded by the constraints explicitly enforced in the MPC formulation. Hence, the proposed approach provides a balanced compromise between tracking accuracy, disturbance rejection, control effort, and control smoothness.

Despite the favourable results, some limitations of the proposed approach should be noted. The use of an augmented state model together with a Kalman filter and an MPC optimization loop increases the computational burden compared to simpler control schemes. In addition, the performance of the method depends on the tuning of weighting matrices and estimator parameters, which may require careful adjustment.

Furthermore, the approach relies on the accuracy of the underlying model. These aspects highlight potential directions for future work, including real-time implementation, robustness analysis under model uncertainties, and the exploration of data-driven extensions. In this context, recent works have highlighted the growing relevance of data-driven and learning-aided MPC schemes for improving prediction accuracy and adaptability in uncertain systems [34].

6. Conclusions

In this paper a novel MPC framework is formulated using a differential flatness-based parametrization of the DC motor–gearhead drive system dynamics, where the gearhead angular velocity is selected as the flat output. Additionally, a Kalman filter scheme with polynomial disturbance estimation enables effective speed tracking under completely unknown load torques. Increasingly demanding simulation scenarios are evaluated while preserving tracking accuracy, disturbance rejection, and control smoothness when compared with conventional LQI and PID controllers, as well as with a nominal offset-free MPC. Several quantitative performance metrics and normalized comparisons confirm that the proposed framework achieves lower tracking errors while maintaining bounded control effort, even in the presence of oscillatory disturbances and measurement noise. A key feature of our proposal is its robustness across operating conditions, since the same MPC parameters and constraints are used in all considered cases, without the need for re-tuning, as the estimation scheme allows the controller to adapt its predictions and control actions to dynamic load torque conditions. Overall, the results demonstrate that an adequate integration of differential flatness, MPC, and Kalman-based online estimation provides a flexible and effective solution for advanced speed control of electric drive systems. Future work will focus on real-time experimental implementation, study on the effect of parameter variations and model uncertainties, as well as a data-driven approach employing the proposed framework along with physics-informed artificial neural networks.

Author Contributions: Conceptualization, E.D.-P., H.Y.-B., F.B.-C., C.S., and D.S.; methodology, E.D.-P., H.Y.-B., F.B.-C., C.S. and D.S.; software, H.Y.-B.; validation, E.D.-P., H.Y.-B., F.B.-C. and J.C.H.; formal analysis, E.D.-P., H.Y.-B., F.B.-C., C.S., D.S. and J.C.H.; investigation, E.D.-P., H.Y.-B., C.S., D.S., F.B.-C. and J.C.H.; resources, J.C.H.; data curation, H.Y.-B.; writing—original draft preparation, E.D.-P.; writing—review and editing, H.Y.-B. and F.B.-C.; visualization, E.D.-P.; supervision, F.B.-C.; project administration, F.B.-C. and J.C.H.; funding acquisition, J.C.H. All authors have read and agreed to the published version of the manuscript.

Funding: This research received no external funding.

Institutional Review Board Statement: Not applicable.

Data Availability Statement: The original contributions presented in this study are included in the article; further inquiries can be directed to the corresponding authors.

Acknowledgments: The authors would like to thank the Secretaría de Ciencia, Humanidades, and Tecnología e Innovación (Secihti) from Mexico, for support provided to developing this work. In addition, the authors gratefully acknowledge the support provided by the Thematic Network 723RT0150, "Red para la Integración a Gran Escala de Energías Renovables en Sistemas Eléctricos [RIBIERSE-Ibero-American Program of Science and Technology for Development (CYTED)]" through the Call for Thematic Networks of the CYTED (Ibero-American Program of Science and Technology for Development), in 2022.

Conflicts of Interest: The authors declare no conflicts of interest.

Abbreviations

The following abbreviations are used in this manuscript:

DC	Direct Current
MPC	Model Predictive Control
LQI	Linear Quadratic Integral
PID	Proportional–Integral–Derivative
ITAE	Integral of Time-weighted Absolute Error
IAE	Integral of Absolute Error

NRMSE Normalized Root Mean Square Error

References

1. Rimpas, D.; Kaminaris, S.D.; Piromalis, D.D.; Vokas, G.; Arvanitis, K.G.; Karavas, C.S. Comparative Review of Motor Technologies for Electric Vehicles Powered by a Hybrid Energy Storage System Based on Multi-Criteria Analysis. *Energies* **2023**, *16*, 2555. [CrossRef]
2. Kuczmann, M. Review of DC Motor Modeling and Linear Control: Theory with Laboratory Tests. *Electronics* **2024**, *13*, 2225. [CrossRef]
3. Manuel, N.L.; İnanç, N.; Lüy, M. Control and performance analyses of a DC motor using optimized PIDs and fuzzy logic controller. *Results Control Optim.* **2023**, *13*, 100306. [CrossRef]
4. Silva-Ortigoza, R.; Marciano-Melchor, M.; García-Chávez, R.E.; Roldán-Caballero, A.; Hernández-Guzmán, V.M.; Hernández-Márquez, E.; García-Sánchez, J.R.; García-Cortés, R.; Silva-Ortigoza, G. Robust Flatness-Based Tracking Control for a Full-Bridge Buck Inverter–DC Motor System. *Mathematics* **2022**, *10*, 4110. [CrossRef]
5. Yañez-Badillo, H.; Beltran-Carbajal, F.; Rivas-Cambero, I.; Favela-Contreras, A.; Arroyo-Nuñez, J.H.; Balderas-Gutierrez, J.N. Enhanced Output Tracking Control for Direct Current Electric Motor Systems Using Bio-Inspired Optimization. *Machines* **2023**, *11*, 1006. [CrossRef]
6. Rawlings, J.B.; Mayne, D.Q.; Diehl, M.M. *Model Predictive Control: Theory, Computation, and Design*, 2nd ed.; Nob Hill Publishing: Madison, WI, USA, 2017.
7. Elmorshedy, M.F.; Xu, W.; El-Sousy, F.F.M.; Islam, M.R.; Ahmed, A.A. Recent Achievements in Model Predictive Control Techniques for Industrial Motor: A Comprehensive State-of-the-Art. *IEEE Access* **2021**, *9*, 58170–58191. [CrossRef]
8. Ghauri, M.A.; Abbasi, M.A.; Shahid, M.B.; Noman, M.; Hakeem, H.M.A. Finite Control Set Model Predictive Field-Oriented Control for Three-Phase Induction Motor Drives. *J. Eng. Res.* **2022** . [CrossRef]
9. Gao, J.; Zhang, J.; Fan, M.; Peng, Z.; Chen, Q.; Zhang, H. Model Predictive Control of Permanent Magnet Synchronous Motor Based on State Transition Constraint Method. *Math. Probl. Eng.* **2021**, *2021*, 3171417. [CrossRef]
10. Shahid, M.B.; Jin, W.; Abbasi, M.A.; Husain, A.R.B.; Munir, H.M.; Hassan, M.; Flah, A.; Souissi, A.S.E.; Alghamdi, T.A.H. Model predictive control for energy efficient AC motor drives: An overview. *IET Electr. Power Appl.* **2024**, *18*, 1894–1920. [CrossRef]
11. Sahin, M. Designing MPC algorithms for velocity control of brushed DC motor and verification with SIL tests. *Automatika* **2023**, *64*, 399–407. [CrossRef]
12. Trivedi, M.S.; Keshri, R.K. Evaluation of Predictive Current Control Techniques for PM BLDC Motor in Stationary Plane. *IEEE Access* **2020**, *8*, 46217–46228. [CrossRef]
13. Li, Z.; Liu, Y.; Tan, W.; Bi, S. Model predictive control for nonlinear system with feedback linearization and extended state observer. *Int. J. Syst. Sci.* **2025** , 1–15. [CrossRef]
14. Son, S.H.; Kim, J.W.; Oh, T.H.; Jeong, D.H.; Lee, J.M. Learning of model-plant mismatch map via neural network modeling and its application to offset-free model predictive control. *J. Process Control* **2022**, *115*, 112–122. [CrossRef]
15. Aouaichia, A.; Stihi, S.; Fareh, R.; Abdul Majid, A.R.; Ghoul, A.; Bettayeb, M.; Kara, K. Neural network model predictive control with active disturbance rejection for robot manipulators trajectory tracking. *J. Frankl. Inst.* **2025**, *362*, 107910. [CrossRef]
16. Schimperna, I.; Toffanin, C.; Magni, L. On offset-free Model Predictive Control with Long Short-Term Memory Networks. *IFAC-PapersOnLine* **2023**, *56*, 156–161. [CrossRef]
17. Zhang, F.; Wang, L. Disturbance rejection design for Gaussian process-based model predictive control using extended state observer. *Comput. Chem. Eng.* **2024**, *186*, 108708. [CrossRef]
18. Li, P.; Su, J.; Wang, H.; Yang, G. Model-free predictive current control of IPMSMs based on an improved extended state observer with parallel resonant controller switching control strategy. *Comput. Electr. Eng.* **2025**, *125*, 110414. [CrossRef]
19. Chen, J.; Dang, Y.; Han, J. Offset-free model predictive control of a soft manipulator using the Koopman operator. *Mechatronics* **2022**, *86*, 102871. [CrossRef]
20. Sun, Z.; Xia, Y.; Dai, L.; Liu, K.; Ma, D. Disturbance Rejection MPC for Tracking of Wheeled Mobile Robot. *IEEE/ASME Trans. Mechatron.* **2017**, *22*, 2576–2587. [CrossRef]

21. Wang, J.; Chen, L.; Xu, Q. Disturbance Estimation-Based Robust Model Predictive Position Tracking Control for Magnetic Levitation System. *IEEE/ASME Trans. Mechatron.* **2022**, *27*, 81–92. [CrossRef]
22. Li, S.; Shi, Y.; Hu, L.; Sun, Z. A generalized model predictive control method for series elastic actuator driven exoskeleton robots. *Comput. Electr. Eng.* **2021**, *94*, 107328. [CrossRef]
23. Muvva, V.V.R.M.K.R.; Joseph, K.T.; Chawla, Y.; Pitla, S.; Wolf, M. Custom UAV with model predictive control for autonomous static and dynamic trajectory tracking in agricultural fields. *Front. Robot. AI* **2025**, *12*, 1694952. [CrossRef] [PubMed]
24. Ghanbarpour, K.; Bayat, F.; Jalilvand, A. An MPC-based fault tolerant control of wind turbines in the presence of simultaneous sensor and actuator faults. *Comput. Electr. Eng.* **2025**, *122*, 109931. [CrossRef]
25. Prasanth, S.; Narayanan, S.; Sivakumaran, N.; Pratheesh, H. The control of superheater steam temperature in power plants using model predictive controller. *Comput. Electr. Eng.* **2024**, *115*, 109109. [CrossRef]
26. Rodriguez-Guevara, D.; Favela-Contreras, A.; Beltran-Carbajal, F.; Sotelo, C.; Sotelo, D. An MPC-LQR-LPV Controller with Quadratic Stability Conditions for a Nonlinear Half-Car Active Suspension System with Electro-Hydraulic Actuators. *Machines* **2022**, *10*, 137. [CrossRef]
27. Fliess, M.; Lévine, J.; Martin, P.; Rouchon, P. Flatness and defect of non-linear systems: Introductory theory and examples. *Int. J. Control* **1995**, *61*, 1327–1361. [CrossRef]
28. Tang, C.; Miller, P.; Krovi, V.; Ryu, J.C.; Agrawal, S. Differential-Flatness-Based Planning and Control of a Wheeled Mobile Manipulator—Theory and Experiment. *IEEE/ASME Trans. Mechatron.* **2011**, *16*, 768–773. [CrossRef]
29. Lu, H.; Liu, C.; Guo, L.; and, W.H.C. Constrained anti-disturbance control for a quadrotor based on differential flatness. *Int. J. Syst. Sci.* **2016**, *48*, 1182–1193. [CrossRef]
30. Rodriguez-Guevara, D.; Favela-Contreras, A.; Beltran-Carbajal, F.; Sotelo, C.; Sotelo, D. A Differential Flatness-Based Model Predictive Control Strategy for a Nonlinear Quarter-Car Active Suspension System. *Mathematics* **2023**, *11*, 1067. [CrossRef]
31. Xu, L.; Tian, B.; Wang, C.; Lu, J.; Wang, D.; Li, Z.; Zong, Q. Fixed-Time Disturbance Observer-Based MPC Robust Trajectory Tracking Control of Quadrotor. *IEEE/ASME Trans. Mechatron.* **2025**, *30*, 4272–4282. [CrossRef]
32. Beltran-Carbajal, F.; Tapia-Olvera, R.; Valderrabano-Gonzalez, A.; Yanez-Badillo, H.; Rosas-Caro, J.; Mayo-Maldonado, J. Closed-loop online harmonic vibration estimation in DC electric motor systems. *Appl. Math. Model.* **2021**, *94*, 460–481. [CrossRef]
33. Beltran-Carbajal, F.; Valderrabano-Gonzalez, A.; Rosas-Caro, J.; Favela-Contreras, A. An asymptotic differentiation approach of signals in velocity tracking control of DC motors. *Electr. Power Syst. Res.* **2015**, *122*, 218–223. [CrossRef]
34. Morato, M.M.; Felix, M.S. Data Science and Model Predictive Control: A survey of recent advances on data-driven MPC algorithms. *J. Process Control* **2024**, *144*, 103327. [CrossRef]
35. Wang, L. *Advances in Industrial Control*; Springer: London, UK, 2009. [CrossRef]
36. Camacho, E.F.; Bordons, C. *Model Predictive Control*, 2nd ed.; Springer: London, UK, 2007.
37. Limouni, T.; Yaagoubi, R.; Bouziane, K.; Guissi, K.; Baali, E.H. A comprehensive review of microgrid control methods: Focus on AI, optimization, and predictive techniques. *Comput. Electr. Eng.* **2025**, *125*, 110442. [CrossRef]
38. Sotelo, D.; Favela-Contreras, A.; Kalashnikov, V.V.; Sotelo, C. Model Predictive Control with a Relaxed Cost Function for Constrained Linear Systems. *Math. Probl. Eng.* **2020**, *2020*, 7485865. [CrossRef]
39. Çelik, D.; Khosravi, N.; Khan, M.A.; Waseem, M.; Ahmed, H. Advancements in nonlinear PID controllers: A comprehensive review. *Comput. Electr. Eng.* **2026**, *129*, 110775. [CrossRef]
40. Muske, K.R.; Badgwell, T.A. Disturbance modeling for offset-free linear model predictive control. *J. Process Control* **2002**, *12*, 617–632. [CrossRef]
41. Simon, D. *Optimal State Estimation: Kalman, H_∞, and Nonlinear Approaches*, 1st ed.; John Wiley & Sons: Hoboken, NJ, USA, 2006.
42. Brown, R.G.; Hwang, P.Y.C. *Introduction to Random Signals and Applied Kalman Filtering: With MATLAB Exercises*, 4th ed.; John Wiley & Sons: Hoboken, NJ, USA, 2012.
43. Ljung, L. *System Identification: Theory for the User*, 2nd ed.; Prentice Hall: Upper Saddle River, NJ, USA, 1999.
44. Goodwin, G.C.; Graebe, S.F.; Salgado, M.E. *Control System Design*; Prentice Hall: Upper Saddle River, NJ, USA, 2001.
45. Anderson, B.D.O.; Moore, J.B. *Optimal Control: Linear Quadratic Methods*; Dover Publications: Mineola, NY, USA, 2007.
46. Åström, K.J.; Hägglund, T. *Advanced PID Control*; ISA—The Instrumentation, Systems, and Automation Society: Research Triangle Park, NC, USA, 2006.
47. Box, G.E.P.; Jenkins, G.M.; Reinsel, G.C.; Ljung, G.M. *Time Series Analysis: Forecasting and Control*, 5th ed.; Wiley: Hoboken, NJ, USA, 2015.